BIFURCATION PHENOMENA IN A THIRD ORDER ELECTRICAL CIRCUIT

by

T. Matsumoto, L. O. Chua and M. Komuro

Memorandum No. UCB/ERL M85/30

22 April 1985

(cover)

BIFURCATION PHENOMENA IN A THIRD ORDER ELECTRICAL CIRCUIT

by

T. Matsumoto, L. O. Chua and M. Komuro

Memorandum No. UCB/ERL M85/30

22 April 1985

ELECTRONICS RESEARCH LABORATORY

College of Engineering
University of California, Berkeley
94720

BIFURCATION PHENOMENA IN A THIRD ORDER ELECTRICAL CIRCUIT

T. Matsumoto
Department of Electrical Engineering
Waseda University, Tokyo 160, Japan

L. O. Chua
Department of Electrical Engineering and Computer Sciences
University of California, Berkeley, CA 94720

M. Komuro
Department of Mathematics
Tokyo Metropolitan University, Tokyo 158, Japan

Key Words : Bifurcation, Electrical Circuit, Chaotic Attractor

Running Title : Bifurcations in Electrical Circuit

ABSTRACT This paper describes the dynamics of the simplest physical system known to date whose chaotic dynamics and rich bifurcation phenomena have been observed not only in the laboratory, but also reconfirmed by extensive computer simulation of its associated mathematical model: a 3rd-order autonomous ordinary differential equation. The physical system is a 5-element electrical circuit whose only nonlinearity is a nonlinear resistor characterized by a 3-segment piecewise-linear voltage-current characteristic.

Despite the simplicity of the circuit, however, it is imbued with an extremely rich variety of bifurcation phenomena. By changing the capacitance values, many phenomena, including Hopf bifurcation, period-doubing cascades, Rössler's spiral-type and screw-type attractors [4], periodic windows, "double-scroll" attractor [1], boundary crisis [5], Shilnikov-type phenomenon [6] etc. have been observed experimentally and confirmed by computer simulation. Other atrractors and periodic windows have also been observed by varying the conductance values.

In addition, Rössler's spiral-type and screw-type attractors have been observed from the same circuit where the nonlinear resistor has only one break point, i.e., it is described by a 2-segment piecewise-linear v-i characteristic. This means that extremely complicated non-periodic (chaotic) waveforms can arise in the simplest third order uncoupled electrical circuit in which all elements except one (a resistor) are linear and passive, and in which the constitutive relation of the nonlinear resistor is made of the simplest conceivable nonlinearity; namely, 2 straight-line segments.

I. INTRODUCTION

This paper reports a great variety of one-parameter bifurcation phenomena observed from the electrical circuit reported in [1]. The circuit is extremely simple : it is third order, autonomous and has no coupling elements[†]. Its only nonlinear element is a 3-segment piecewise-linear[††] resistor. Even though the circuit is simple, very rich bifurcation phenomena have been observed. In Section II, bifurcation phenomena observed experimentally by varying the capacitance values are shown. In Section III, we confirm our experimental observations with digital computer simulations. Moreover, our simulation analysis reveals that the observed phenomena exhibit Hopf bifurcation, cascades of period doubling, Rössler's spiral-type and screw-type attractors [4], periodic windows, "double-scroll" attractor [1], boundary crisis [5], and a Shilnikov-type phenomenon [6].

In addition, Rössler's spiral-type and screw-type attractors have also been observed from the same circuit but with the constitutive relation of the nonlinear resistor further simplified to have only one break point, i.e., it is described by a continuous 2-segment piecewise-linear function. The chaotic attractor associated with this even simpler circuit is confirmed experimentally as well as numerically. These observations show that the extremely complicated non-periodic (chaotic) waveforms can arise in the simplest third-order uncoupled circuit in which all elements except one (a resistor) are linear and passive, and in which the nonlinear resistor is almost linear : its incremental resistance assumes only two values.

We emphasize in this paper that our circuit is a physical system, and not an analog computer. The simplicity of our circuit, allows us to

---

† Such a circuit is called reciprocal [2], [3]. Physically, this means that the constitutive relations of the circuit elements are potential functions.

†† Piecewise-linearity simplifies the realization of the circuit (Fig.2) in a significant manner. It also helps greatly in visualizing the structure of the attractor [1].

build it easily and hence carefully controlled laboratory experiments can be carried out in a very simple manner. Extensive numerical simulations are used not only to validate the following differential equations used to model our physical circuit, but also to determine the bifurcation parameter values with much greater resolution than is possible by measurements.

Let us first recall the circuit reported in [1]. Figure 1(a) gives the circuitry while Fig. 1(b) shows the constitutive relation; i.e., the v-i characteristic, of the nonlinear resistor†. The dynamics is described by

$$\begin{aligned} C_1 \frac{dv_{C_1}}{dt} &= G(v_{C_2} - v_{C_1}) - g(v_{C_1}) \\ C_2 \frac{dv_{C_2}}{dt} &= G(v_{C_1} - v_{C_2}) + i_L \\ L \frac{di_L}{dt} &= - v_{C_2} \end{aligned} \tag{1.1}$$

where the function g(.) is given by Fig. 1(b) and

$$\begin{cases} 1/C_1 = 9,\ 1/C_2 = 1,\ 1/L = 7,\ G = 0.7 \\ m_0 = -0.5,\ m_1 = -0.8,\ B_p = 1. \end{cases} \tag{1.2}$$

In Section II and Section III, the capacitance C_1 is chosen as the bifurcation parameter while the other parameters are held fixed as in (1.2). In Section IV, the conductance G is chosen as the bifurcation parameter.

II. THE CAPACITANCE BIFURCATIONS

In order to observe the C_1 bifurcations, we set up the circuit of Fig. 2(a) which realizes the circuit of Fig. 1 (with appropriate scaling). The subcircuit inside the broken-line box N realizes the function g(·) of Fig. 1(b). Figure 2(b) shows the measured v-i characteristic. Starting

† The symbol for the nonlinear resistor is a standard one among the circuit theory community.

with 6130 pF we slowly adjusted the value of C_1 and reduced it to 5400 pF. Figure 3 shows several of the observed attractors projected onto the (i_L, v_{C_1})-plane, in the order of decreasing C_1. For large values of C_1, we observed nothing but a point, i.e., all the trajectories settled down to a stable equilibrium. After decreasing C_1 by an appropriate amount, we observed that a periodic attractor (stable limit cycle) was born (Fig. 3(a)). Then period doubling was initiated (Fig. 3(b), (c)). Figure 3(c) is blown up in Fig. 3(d), where the period-4 nature is easier to see. Further period doubling was difficult to observe. (Recall that the sequence of parameter values at which further period doubling occurs converges to a limit very rapidly [7].) In Fig. 3(e), the attractor does not appear to be periodic any more. It seems to have the structure of a Rössler's spiral-type attractor [4]. In Section III, we will confirm this observation with digital simulation.

Upon further decreasing C_1, we observed the periodic window† of Fig. 3(f). After this, the attractor again became non-periodic (Fig. 3(g)). In Section III, we will explain, via digital simulation, that this appears to be a Rössler's screw-type attractor [4]. Now recall that the dynamics (1.1) is symmetric with respect to the origin. Therefore, in Fig. 3(a) - (g), there should be a "twin" attractor located symmetrically with respect to the origin. Indeed, by switching on and off the power supply for the operational amplifier (thereby changing the initial conditions) we have observed both attractors. Further decrease of C_1 gave birth to an interesting new phenomenon. The attractor suddenly doubled its size and became symmetric itself with two "holes" (Fig. 3(h)). The two independent attractors seemed to have collided with each other and emerged as a single attractor. This is the "double-scroll"

---

† A periodic window is understood to be a brief interval in the bifurcation parameter where the solution is a periodic attractor but becomes chaotic outside of the interval [8]. Even though this has been used for 1-dimensional maps [8], it applies equally well for flows in a natural manner.

attractor carefully analyzed and described in great detail in [1].

After this, the two holes became smaller and smaller, and the intensity of the trajectory near the holes became notably high (Fig. 3(i)). This means that the trajectory spends more time near the holes than in the other parts of attractor. In Section III we will explain, via simulation, that this trajectory is in the verge of evolving into a Shilnikov-type phenomenon [6]. Here a Shilnikov-type phenomenon is to be interpreted as the existence of a pair of heteroclinic trajectories which, in turn, implies the existence of infinitely many saddle-type periodic orbits in every neighborhood of the heteroclinic trajectory (see Section III). Next, we have observed the periodic window of Fig. 3 (j) after which we saw again chaotic attractors similar to those in Fig. 3 (h) and (i). As we further decreased C_1, however, the attractor suddenly disappeared. We will show, in Section III, that this corresponds to a boundary crisis [5], i.e., an attractor suddenly disappears when it touches an unstable periodic orbit.

Although we have observed periodic windows which are more bizarre than Fig. 3(f) and (j), we omit them to conserve space.

Figure 4(a), (b) and (c) show the time waveforms of $v_{C_1}(t)$, $v_{C_2}(t)$ and $i_L(t)$, respectively corresponding to Fig. 3(h). Note that the waveform of $v_{C_2}(t)$ is unbiased, (i.e., no dc component) since the v_{C_2}-component of the equilibra of (1.1) is always zero. (see Section III).

The usage of the word "chaotic attractor" is of course not rigorous in this paper as well as in other papers in the sense that a mathematical proof of its existence is not given.† However, we have given a physical evidence by designing and building a physical circuit whose equation of motion is

---

† It has been often argued that "chaotic attractors" observed by digital simulation are of questionable validity because of local truncation and round off errors.

modelled by (1.1)†. We cannot overemphasize, that the circuit of Fig. 2 is not an analog computer in the sense that its building blocks are not integrators.†† They are ordinary circuit elements; namely, resistors, inductors and capacitors. Both current and voltage of each circuit element play a crucial role in the dynamics of the circuit. On the contrary, the variables in a typical analog computer are merely node voltages of the capacitor-integrator building-block modules where the circuit current is completely irrelevant in the circuit's dynamic operation. Hence it would be misleading to confuse our circuit as an analog computer. Indeed, any abstraction or generalization of the term "analog computer" on our circuit would imply that all physical circuits, or for that matter all physical systems, are analog computers, which is absurd.

We close this section by giving several circuit theoretic explanations of the chaotic behavior of our circuit in Fig. 1 (a). First note that the parallel connection (tank circuit) of C_2 and L constitutes one basic oscillatory mechanism in the (v_{C_2}, i_L)-plane, whereas the conductance G provides the interactions between the (C_2, L)- oscillatory component and the "active" [2] resistor $g(\cdot)$ together with C_1. This active resistor is of course responsible for the circuit's chaotic behavior. If this resistor were locally passive [2], it is well known that the circuit would be quite tame : all solutions would approach a globally asymptotically stable equilibrium [9]. Since

---

† Of course, due to component tolerances, the physical circuit in Fig. 2 is not exactly modelled by (1.1). However, the fact that this circuit exhibits an almost identical attractor on an oscilloscope shows that (1.1) is indeed a robust model.

†† There is a tendency for readers outside of electronic circuit theory to associate an operational amplifier with an electronic analog computer. The operational amplifier in the circuit N of Fig. 2(a) is used for an entirely different purpose: to realize the constitutive relation (Fig. 1(b)) of the nonlinear resistor. In fact, one could eliminate the operational amplifier and realize N by an integrated circuit (made of bipolar transistors and diodes) encapsulated in a standard package just like any other garden variety IC components.

$g(\cdot)$ is always locally active [2], i.e., $v_R(t)\, i_R(t) < 0$ (except at the origin) it keeps supplying power to the external circuit. The attracting nature of the chaotic trajectories comes from the power dissipation in the passive element G, thereby restraining its growth. The power balance, however, is rather delicate, and varies continuously with time, but never repeating itself periodically except for parameter values which resulted in a periodic oscillation.

III. NUMERICAL CONFIRMATION

In this section, we will confirm, via digital simulation, the bifurcation phenomena observed from the physical circuit in the previous section.

First consider the equilibria of (1.1) :

$$G(v_{C_2} - v_{C_1}) - g(v_{C_1}) = 0$$

$$G(v_{C_1} - v_{C_2}) + i_L = 0$$

$$v_{C_2} = 0 \quad .$$

Therefore, for fixed values of G, m_0 and m_1 given by (1. 2), there are three equilibria :

$$\underset{\sim}{P}^+ : \quad v_{C_1} = k, \; v_{C_2} = 0, \; i_L = - Gk$$

$$\underset{\sim}{Q} : \quad v_{C_1} = v_{C_2} = i_L = 0$$

$$\underset{\sim}{P}^- : \quad v_{C_1} = - k, \; v_{C_2} = 0, \; i_L = G k$$

where k and - k are the positive and negative solutions of

$$G \, v_{C_1} + g(v_{C_1}) = 0 \quad .$$

One can show that for any $C_1 > 0$, the origin is unstable (see the APPENDIX). The other two equilibria change their stability type as C_1 varies.

A. Hopf Bifurcation

Using the Routh formula (see the APPENDIX), one can show that for

$$1/C_1 \; < \; \frac{1}{2} \left(-3.5 + \sqrt{(3.5)^2+280} \; \right) \approx 6.8$$

$\underset{\sim}{P}^+$ and $\underset{\sim}{P}^-$ are stable. At

$$1/C_1 = \frac{1}{2}\left(- 3.5 + \sqrt{(3.5)^2+280}\ \right)$$

a pair of eigen values crosses the imaginary axis and a Hopf bifurcation occurs [6], [10], thereby signifying the birth of a periodic orbit. Hopf bifurcation here, however, should be interpreted in its generalized sense, because the right hand side of (1.1) is only continuous but not a C^4 function†. Figure 5 shows two distinct periodic attractors (stable limit cycles) at

$$1/C_1 = 8.0.$$

Compare this with Fig. 3(a) and recall that the periodic attractors occur in pairs because of the symmetry of (1.1).

B. Period Doubling

As we increase $1/C_1$ slightly beyond 8.0, a period-doubling bifurcation is initiated. Figure 6 shows the period-2 attractors at (compare with Fig. 3(b))

$$1/C_1 = 8.2$$

while Fig. 7 (compare with Fig. 3(c),(d)) shows two period-4 attractors at

$$1/C_1 = 8.44.$$

Any further period doubling was difficult to observe.

C. Rössler's Spiral-type Attractor

At

$$1/C_1 = 8.5$$

the attractor in Fig. 8 no longer appears to be periodic (compare with

---

† The same phenomena, however, can be observed by approximating the right hand side of (1.1) by a C^∞ function.

Fig. 3(e)). It has the structure of a Rössler's spiral-type attractor [4]. If one chooses an initial condition on the attractor, then the trajectory starts rotating outwards in a counterclockwise direction around the hole, thereby receding further and further away from the center of the hole, i.e., the point where $\underset{\sim}{P}^+$ or $\underset{\sim}{P}^-$ is located. After a certain random time interval, however, the trajectory returns to a point closer to $\underset{\sim}{P}^+$ or $\underset{\sim}{P}^-$ and then repeats a similar process.

As was explained earlier, the symmetry of (1.1) implies that there is another spiral-type attractor located symmetrically with respect to the origin. The symmetry, in turn, stems from the symmetry of the function $g(\cdot)$ in Fig. 1(b). This observation suggests that one attractor should still be present even if one replaces the 3-segment function of Fig. 1(b) with the 2-segment function in Fig. 9. This conjecture is confirmed in Fig. 10, where the spiral-type attractor is observed with a piecewise-linear resistor having only one break point. This has been confirmed experimentally also. Note that the circuit has no coupling elements. Sparrow [11] and Rössler et. al. [12] had also observed non-periodic attractors from piecewise-linear systems with only one break point. Their systems, however, do not appear to be realizable by circuits without coupling elements, and are therefore more complicated from a circuit theory point of view.

As we continue tuning the bifuration parameter C_1, we observed that the spiral-type attractor persists up to

$$1/C_1 \quad \underset{\approx}{<} \quad 8.575.$$

D. Periodic Window

At

$$1/C_1 \quad \approx \quad 8.575$$

a periodic window of Fig. 11 has been observed (compare with Fig. 3(f)). After this, a spiral-type attractor is observed again.

E. Rössler's Screw-type Attractor

As we increase $1/C_1$ further the above spiral-type attractor eventually deforms into a Rössler's screw-type attractor [4] where the trajectory sometimes makes more than one rotations before completing its descent. Figure 12 shows this attractor at

$$1/C_1 = 8.8066.$$

Of course, there is another screw-type attractor located symmetrically with respect to the origin. We have omitted the other attractor to avoid the trajectories of the two attractors from entangling each other, which they don't (at this parameter value) in the 3-dimensional state space. Observe that Fig. 3(g) appears to be a screw-type attractor. In Fig.3(g), however, it is not easy to detect the "screw" structure of this attractor because the associated trajectory does not make more than one rotations before completing its descent very often.

F. Double-Scroll Attractor

As we increase $1/C_1$ further, the attractor abruptly enlarges itself and creates two holes located symmetrically with respect to the origin. The two attractors of Fig. 12 have collided with each other as was described in Section II. It then evolves quickly into Fig. 13 (compare with Fig. 3(h)) which corresponds to the parameter value

$$1/C_1 = 9.0 \ .$$

This is the "double-scroll" attractor described in [1], where it is shown that two sheet-like objects are curled up together many times. If one chooses an initial condition near the "upper hole", then the trajectory starts rotating outwards in a counterclockwise direction around the hole. After a certain random interval, the trajectory sometimes returns to a point closer to the upper hole. At some other times, however, it starts descending with respect to the v_{C_1}-axis in a spiral path and "lands" at a point near the "lower hole".

It then starts rotating outwards in a counterclockwise direction around the lower hole. As expected (due to symmetry), the behavior after this descent is similar to the spiral excursion around the upper hole.

This attractor appears to persist over the parameter interval

$$8.81 \lesssim \quad 1/C_1 \quad \lesssim \quad 10.05.$$

However, at the parameter value

$$1/C_1 \; = 10.05$$

the periodic window of Fig. 14 is observed (compare with Fig. 3 (j)). After this, several other strange-looking windows (not shown) have been seen.

G. Shilnikov-type Phenomenon

Another interesting phenomenon is observed at the parameter value

$$1/C_1 \; \approx \; 9.78$$

where a trajectory with an initial condition on the unstable manifold $W^u(\underset{\sim}{P}^-)$ of $\underset{\sim}{P}^-$ flows into the stable manifold $W^s(\underset{\sim}{P}^+)$ of $\underset{\sim}{P}^+$. Since (1.1) is symmetric with respect to the origin, a trajectory starting from the unstable manifold $W^u(\underset{\sim}{P}^+)$ of $\underset{\sim}{P}^+$ would eventually flow into the stable manifold $W^s(\underset{\sim}{P}^-)$ of $\underset{\sim}{P}^-$ also. This is shown in Fig. 15 (compare with Fig. 3(i))†. Hence there would be a pair of heteroclinic orbits between $\underset{\sim}{P}^+$ and $\underset{\sim}{P}^-$. The eigen values at $\underset{\sim}{P}^{\pm}$ consist of a complex conjugate pair

$$\sigma \pm j\omega \; \approx \; 0.17 \; \pm \; j \; 2.13$$

in the right half plane, and a real number

$$\gamma \; \approx \; - \; 2.30$$

in the left half plane. Since

$$\sigma \; < \; | \; \gamma \; |$$

we can invoke Shilnikov's theorem [6] to conjecture that there are infinitely

---

† Of course, numerical error prevents any computer from showing this phenomenon exactly. One can observe, however, that the trajectory almost hits $\underset{\sim}{P}^+$ and spends an extremely long period of time near $\underset{\sim}{P}^+$.

many saddle-type periodic orbits in every neighborhood of these heteroclinic orbits.†

H. Boundary Crisis

Figure 16 shows the attractor at

$$1/C_1 = 10.5.$$

Suddenly, however, at

$$1/C_1 \approx 10.75$$

the attractor disappears: equation (1.1) diverges with any initial condition!. This disappearing act provokes the interesting question as to how the attractor dies. A careful analysis suggests that this phenomenon is related to the simultaneous presence of a saddle-type closed orbit encircling the attractor. To see this, let us go back to the parameter value $1/C_1 = 8.0$. With this value, a saddle-type closed orbit has been found outside the periodic attractors. It is shown by the broken closed curve in Fig. 17. Since this orbit is not attracting, one cannot observe it on an oscilloscope. Nor can one observe it with a digital computer by integrating backward in time since it is saddle-type. Newton iteration and "Shooting Method" were used to find it. As we increase $1/C_1$, the saddle-type periodic orbit shrinks gradually as shown in Figs. 18-22. At $1/C_1 = 10.5$, the attractor is located very close to the saddle-type periodic orbit (Fig. 23). With a slight increase in $1/C_1$ beyond 10.5, the attractor appears to collide with the saddle type periodic orbit. This collision provides a natural mechanism leading to the attractor's death. Note that if the attractor stays away from the saddle-type closed orbit, there would be no way for the trajectory in the attractor to escape. Figure 24 shows the situation at $1/C_1=9.0$. The square in the upper left-hand corner is the Poincare section $v_{C_2} = 0$ and the arrows indicate the stable and unstable

† Shilnikov's theorem assumes a homoclinic orbit. His result, however, can be extended to apply to our present situation.

eigin spaces of the Poincare map. This picture is looked at from an angle different from that of the other figures in order to show the relative positions of various sets. Now if the attractor collides with the saddle-type closed orbit, then it would provide an exit path for the trajectory to escape into the outer space. This is what happens at $1/C_1 \approx 10.75$. After this, no attractor can be detected. The attractor seems to be "quenched" upon colliding with the saddle-type closed orbit.

The distinct phenomenon observed at $1/C_1 \approx 10.75$ clearly corresponds to the boundary crisis [5] defined for 1-dimensional maps, i.e., an attractor suddenly disappears when it touches an unstable periodic point. This observation raises another interesting question: Does the saddle-type closed orbit also die when it collides with the attractor? The answer is negative. It survives even after the attractor's death. Figure 25 shows the saddle-type closed orbit at

$$1/C_1 = 13.0.$$

Although this orbit appears to be pinched at the center, it really is a simple (i.e., non-intersecting) closed curve in the 3-dimensional state space.

The saddle-type closed orbit keeps shrinking in size while its period gets longer and longer as one increases $1/C_1$. So far we have observed that the saddle-type closed orbit persists for parameter values up to $1/C_1 = 13.0$. It would be interesting to determine whether this saddle-type closed orbit would eventually bifurcate into some other object at some larger value of $1/C_1$ or, whether it would survive for all values of $1/C_1$. To carry out this analysis, however, would not be easy because there would be other saddle-type periodic orbits (those which "grew" out of the chaotic attractor) coexisting very close to the one we have been tracking as we increase $1/C_1$. Although we have observed such coexistence phenomena, we will not elaborate further on it since it is outside the scope of this paper.

I. Summary

Table 1 summerizes the sequence of bifurcations described above where the types of the eigen values at the three equilibria are also given. (Recall that the nonlinearity in (1.1) is a 3-segment piecewise-linear function and that each linear region can have at most one equilibrium. Hence the dynamics is strongly influenced by the eigen values at the equilibria.) Each equilibrium has a pair of complex conjugate eigen values $\sigma \pm j\omega$ and a real eigen value γ.

The above observations naturally suggest one method for quenching chaos: If one increases the value of C_1 by a sufficiently large amount, then the circuit would not be chaotic. If, on the other hand, one decreases the value of C_1, then the circuit tends to diverge with any initial condition. If the function $g(\cdot)$ is eventually passive†, e.g. Fig. 26, small values of C_1 would cause the trajectories to converge to a large stable limit cycle as described in [1]. In fact, the eventual saturation of the operational amplifier for large output voltages naturally gives rise to eventual passivity. It saturates, however, in a region far beyond the region where the chaotic attractors are located.

We have found that one parameter bifurcations of C_2 and L are qualitatively similar to those of C_1. Chaos can also be quenched by either increasing or decreasing the value of C_2 or L.

---

† A resistor characteristic $i_R=g(v_R)$ is said to be eventually passive [2] if $v_R g(v_R) > 0$ for $|v_R|$ sufficiently large, i.e., it eventually dissipates power.

IV THE CONDUCTANCE BIFURCATIONS

In this section we fix C_1, C_2, L, m_0 and m_1 as in (1.2) and vary G. To conserve space, we will give only numerical observations in this section even though the G bifurcation phenomena have also been experimentally observed from the circuit of Fig. 2.

Recall that $m_0 = -0.5$, $m_1 = -0.8$ and observe that for

$$|m_0| < G < |m_1|$$

there are three equilibria ($\underset{\sim}{Q}$, $\underset{\sim}{P}^+$ and $\underset{\sim}{P}^-$). If, however,

$$0 < G \leq |m_0|$$

or if

$$|m_1| < G$$

then the origin is the only equilibrium. We will exclude the cases G=0 and $G = |m_1|$, since the former is trivial and the latter gives rise to infinitely many equilibria. This stems from the fact that $g(\cdot)$ is piecewise-linear. It is not, however, an essential restriction to our analysis here.

Table 2 together with Fig. 27 - Fig. 43 shows the sequence of conductance bifurcation phenomena.

For $0 < G \leq 0.5 = |m_0|$, the origin is the only equilibrium and it is unstable: no attractor is observed. For $0.5 < G \lessapprox 0.606$, $\underset{\sim}{P}^+$ and $\underset{\sim}{P}^-$ are sinks, while $\underset{\sim}{Q}$ is unstable. Here, our computer simulation shows all trajectories approach either $\underset{\sim}{P}^+$ or $\underset{\sim}{P}^-$.

At $G \approx 0.607$ Hopf bifurcation occurs and a stable periodic orbit is born around $\underset{\sim}{P}^+$ and $\underset{\sim}{P}^-$ (Fig. 27). Here and after, only one of the symmetric pair will be shown. Period doubling cascade, then, takes place (Fig. 28 - Fig. 29). At $G \approx 0.65$, a spiral-type attractor is seen (Fig. 30). At $G \approx 0.68$ the two attractors collide with each other as in the previous sections and a double-scroll attractor is observed (Fig. 31).

The double-scroll attractor persists up to $G \approx 0.7497$ but at $G \approx 0.7498$ a periodic window of Fig. 32 is seen. Since this periodic attractor is

asymmetric whereas (1.1) is symmetric with respect to the origin, another periodic attractor located symmetrically with respect to the origin must also be present. At $G \approx 0.75$ a "period-2" version of the preceding orbit is seen (Fig. 33). From the computer graphics terminal, this period-2 orbit looks like a string which winds around twice before returning to any starting point. At $G \approx 0.751$, the orbit no longer appears to be periodic but keep winding around ("infinitely") many times, forming a thin "ribbon-like" attractor (Fig. 34). Since this is asymmetric with respect to the origin, another "ribbon" exists simultaneously. At $G \approx 0.753$ an object similar to Fig. 32 is obtained (Fig. 35). For $0.7535 \lesssim G \lesssim 0.766$, a periodic window is again observed (Fig. 36). For $0.766 \lesssim G \lesssim 0.7694$ a double-scroll attractor reappears (Fig. 37).

At $G \approx 0.7694$ the double-scroll attractor splits into two parts and a pair of "split ribbons" is observed as shown in Fig. 38 (only one ribbon is shown). At $G \approx 0.77$ another periodic attractor is observed (Fig. 39). At $G \approx 0.773$ a spiral-type attractor reappears (Fig. 40).

Beyond $G \approx 0.784$, a reverse period doubling (i.e., period halving) cascade takes place (Fig. 41 - Fig. 43).

It is interesting to observe that for $0.8 \lesssim G \lesssim 0.817$ the origin is a sink. At $G \simeq 0.817$ the complex conjugate pair of eigen values associated with the origin crosses the imaginary axis beyond which (1.1) diverges with any initial condition except the origin.

Table 1

Summary of C_1 Bifurcation Phenomena

$1/C_1$	Eigen Values complex : $\sigma \pm j\omega$ real : γ		Description of Dynamics	Figure
	$\underset{\sim}{Q}$	$\underset{\sim}{P}^{\pm}$		
$0 < 1/C_1 < 6.8$		$\sigma<0$, $\gamma<0$	$\underset{\sim}{P}^{\pm}$ are sinks	
6.8		$\sigma=0$, $\gamma<0$	Hopf at $\underset{\sim}{P}^{\pm}$	
$6.8 < 1/C_1 < 8.2$			periodic around $\underset{\sim}{P}^{\pm}$	5
8.2	$\sigma < 0$		period 2	6
8.44		$\sigma > 0$	period 4	7
8.5	$\gamma > 0$		spiral-type	8
8.575		$\gamma < 0$	periodic window	11
8.8066			screw-type	12
$8.81 < 1/C_1 < 10.05$			double-scroll	13
10.05			periodic window	14
9.78			Shilnikov-type	15
10.75			crisis	(16)†
$10.75 < 1/C_1$			diverges from any initial condition	

† Figure 16 is obtained at $1/C_1 = 10.5$ which does not yet give rise to a crisis. It is close to it, however.

Table 2

Summary of G Bifurcation Phenomena

G	Eigen Values complex : $\sigma \pm j\omega$ real : γ		Description of Dynamics	Figure
	$\underset{\sim}{0}$	$\underset{\sim}{P}^{\pm}$		
$0 < G \leqq 0.5$			diverges from any initial condition	
$0.5 < G < 0.606$		$\sigma<0$, $\gamma<0$	$\underset{\sim}{P}^{\pm}$ are sinks	
0.606		$\sigma=0$, $\gamma<0$	Hopf at $\underset{\sim}{P}^{\pm}$	
$0.606 < G < 0.64$			periodic around $\underset{\sim}{P}^{\pm}$	27
0.64			period 2	28
0.645			period 4	29
0.65	$\sigma < 0$	$\sigma > 0$	spiral-type	30
$0.68 \leqq G < 0.7498$	$\gamma > 0$	$\gamma < 0$	double-scroll	31
0.7498			periodic	32
0.75			period 2	33
0.751			"ribbon"	34
0.753			period 2	35
$0.753 < G < 0.766$			periodic	36
$0.766 \leqq G < 0.7694$			double-scroll	37
0.7694			"ribbon"	38
0.77			periodic	39
0.773			spiral-type	40
0.784			period 4	41
0.785			period 2	42
$0.795 \leqq G < 0.8$			periodic	43
$0.8 < G < 0.817$	$\sigma<0$, $\gamma<0$		$\underset{\sim}{0}$ is a sink	
0.817	$\sigma=0$, $\gamma<0$		Hopf at $\underset{\sim}{0}$	
$0.817 \leqq G$	$\sigma>0$, $\gamma<0$		diverges from any initial condition	

APPENDIX

The characteristic equation at an equilibrium is given by

$$f(\lambda) \triangleq \lambda^3 + a_1 \lambda^2 + a_2 \lambda + a_3 \tag{A.1}$$

where

$$\begin{aligned} a_1 &= (G + Dg)/C_1 + G/C_2 \\ a_2 &= (G\, Dg/C_1 + 1/L)/C_2 \\ a_3 &= (G + Dg)/(C_1 C_2 L) \end{aligned} \tag{A.2}$$

and Dg denotes the derivative of $g(\cdot)$ Recall that the Routh array [13] is given by

$$\begin{bmatrix} 1 & a_2 \\ a_1 & a_3 \\ a_2 - a_3/a_1 & \cdot \\ a_3 & \cdot \end{bmatrix}$$

and that an equilibrium is stable <u>if and only if</u>

$$a_1,\ a_2,\ a_3,\ a_2 - a_3/a_1 > 0\ . \tag{A.4}$$

At the origin Dg= - 0.8 and G=0.7 so that

$$a_3 < 0$$

for all C_1, hence the origin is always unstable. At $\underset{\sim}{P}^+$ and $\underset{\sim}{P}^-$, however, Dg= -0.5 and (A.4) can be satisfied depending on the value of $1/C_1$. With the values of C_2, L, m_0, m_1, B_p, G fixed as in (1.2), one can explicitly compute the value of $1/C_1$ for which $\underset{\sim}{P}^+$ and $\underset{\sim}{P}^-$ loose their stability. Note that a_1, a_2 and a_3 of (A.2) and $a_2 - a_3/a_1$ are given by

$$\begin{aligned} a_1 &= (0.7-0.5)/C_1 + 0.7 \\ a_2 &= (-0.7 \times 0.5)/C_1 + 7 \\ a_3 &= 7(0.7-0.5)/C_1 \\ a_2 - a_3/a_1 &= 7 - 0.35/C_1 - \frac{1.4/C_1}{0.7 + 0.2/C_1}\ . \end{aligned}$$

For small $1/C_1$, (A.4) is satisfied. It can easily be checked that as one increases $1/C_1$, the first inequality violated is the last one. Therefore,

one looks for a positive real solution to

$$a_1 a_2 - a_3 = 0 \qquad (A.5)$$

which is

$$1/C_1 = \frac{1}{2}\left(-3.5 + \sqrt{(3.5)^2+280}\right) \triangleq 1/C_1^*.$$

In order to see that (A.5) is equivalent to the fact that $\sigma = 0$, i.e., that there is a pair of pure imaginary eigen values, observe that

$$f(\lambda) = (\lambda-\gamma)\ (\lambda-(\sigma + j\omega))\ (\lambda-(\sigma - j\omega))$$

and (A.1) imply

$$a_1 = -(2\sigma + \gamma)$$

$$a_2 = \sigma^2 + \omega^2 + 2\sigma\gamma$$

$$a_3 = -\gamma\ (\sigma^2 + \omega^2).$$

Since

$$a_1\ a_2 - a_3 = -2\sigma\ ((\sigma + \gamma)^2 + \omega^2)$$

one sees that (A.5) is equivalent to

$$\sigma = 0$$

i,e., there is a pair of pure imaginary eigen values. Now recall that for $1/C_1 < 1/C_1^*$ (A.4) holds. On the other hand, one can show that for $1/C_1 = 1/C_1^* + \delta$, and $\delta > 0$ small, we have

$$a_1,\ a_2,\ a_3 > 0, \text{ but } a_2 - a_3/a_1 < 0$$

i.e., the first column of the Routh array changes the sign of its components twice. Therefore, with $1/C_1 = 1/C_1^* + \delta$, $\delta > 0$ small, there are two unstable eigenvalues.

ACKNOWLEDGEMENT We would like to thank S. Tanaka, M. Kurokawa, K. Kobayashi, H. Tomonaga, R. Tokunaga and K. Tokumasu of Waseda University for discussions.

This work has been supported in part by a Grant in Aid of the Japanese Ministry of Education, the Saneyoshi Foundation, the Institute of Applied Electricity, the Institute of Science and Engineering and Tokutei Kadai of Waseda University, and the ONR under contract N00014-70-C-0572.

REFERENCES

[1] T. Matsumoto, L.O. Chua and M. Komuro, IEEE Trans. CAS, Aug. 1985 in press.

[2] L.O. Chua, IEEE Trans. CAS, CAS-27 (1980) 1059.

[3] R.K. Brayton and J.K. Moser, Quart. Appl. Math. 22 (1964) 1 and 81.

[4] O.E. Rössler, Ann. N.Y. Aca. Sci., 31, (1979) 376.

[5] C. Grebogi, E. Ott and J. Yorke, Phys. Rev. Lett., 48, (1982) 1507.

[6] J. Guckenheimer and P. Holmes, Nonlinear Oscillations, Dynamical Systems, and Bifurcations of Vector Fields, (Springer, New York, 1983).

[7] M. J. Feigenbaum, Los Alamos Science, Summer (1980) 4.

[8] R. M. May, Nature, 261 (1976) 459.

[9] L.O. Chua and D.N. Green, IEEE Trans. CAS, CAS-23 (1976) 292.

[10] A.I. Mees and L.O. Chua, IEEE Trans. CAS, CAS-26 (1979) 235.

[11] C.T. Sparrow, J. Math. Anal. Appl., 83 (1981) 275.

[12] O.E. Rössler, C. Kahlert and B. Uehleke, preprint.

[13] E.J. Routh, Dynamics of a System of Rigid Bodies (Macmillan, London, 1905).

FIGURE CAPTIONS

Fig. 1 Simple uncoupled circuit with chaotic attractors. (a) Circuitry. (b) Nonlinear resistor v-i characteristic.

Fig. 2 Physical realization of the circuit in Fig. 1. (a) Circuitry which realizes (1.1) with appropriate scaling. Subcircuit in the broken-line box N realizes g (•) of Fig. 1(b). (b) Measured function g(•). Horizontal scale : 2V/division. Vertical scale : 2mA/division.

Fig. 3 Attractors observed with the circuit of Fig. 2 projected onto the (i_L, v_{C_1})-plane. Horizontal scale (except (d)) : 2mA/division. Vertical scale (except (d)) : 2V/division. In (a) - (g) only one of two attractors is shown. (a) Periodic orbit shortly after Hopf bifurcation. (b) Period-2 orbit. (c) Period-4 orbit. (d) Blown up version of (c). Horizontal scale : 1mA/division. Vertical scale : 1 V/division. (e) Rössler's spiral-type attractor. (f) Periodic window. (g) Trajectory near Rössler's screw-type attractor. (h) "Double-Scroll" attractor. (i) Trajectory near a Shilnikov-type phenomenon. (j) Periodic window.

Fig. 4 Waveforms of state variables corresponding to Fig. 3(h).
(a) v_{C_1}. Horizontal scale : 0.5 msec/division. Vertical scale : 2V/division.
(b) v_{C_2}. Horizontal scale : 0.5 msec/division. Vertical scale : 2V/division.
(c) i_L. Horizontal scale : 0.5 msec/division. Vertical scale: 5mA/division.

Fig. 5 Pair of periodic orbits projected onto the (i_L, v_{C_1})-plane at $1/C_1 = 8.0$. Here and after, the length of each arrow along each axis is 2.0.

Fig. 6 Pair of period-2 orbits at $1/C_1=8.2$.

Fig. 7 Pair of period-4 orbits at $1/C_1=8.44$.

Fig. 8 Pair of Rössler's spiral-type attractor at $1/C_1= 8.5$.

Fig. 9 Modified resistor characteristic with a single break point.

Fig. 10 Spiral-type attractor obtained with the nonlinear resistor characteristic of Fig. 9 ($1/C_1= 8.5$).

Fig. 11 Periodic window at $1/C_1=8.575$.

Fig. 12 Rössler's screw-type attractor at $1/C_1= 8.8066$. To avoid confusion, another screw-type attractor located symmetrically with respect to the origin is omitted.

Fig. 13 "Double-Scroll" attractor at $1/C_1=9.0$.

Fig. 14 Periodic window at $1/C_1=10.05$.

Fig. 15 Shilnikov-type phenomenon observed at $1/C_1=9.78$.

Fig. 16 Attractor at $1/C_1=10.5$.

Fig. 17 Periodic orbits of Fig. 5 together with the saddle-type periodic orbit ($1/C_1=8.0$). Length of the arrow along each axis is still 2.0 even though the scale of the figure is different from that of Fig. 5.

Fig. 18 Period-2 orbits of Fig. 6 together with the saddle-type periodic orbit ($1/C_1=8.2$).

Fig. 19 Period-4 orbits of Fig. 7 together with the saddle-type periodic orbit ($1/C_1=8.44$).

Fig. 20 Spiral-type attractors of Fig. 8 together with the saddle-type periodic orbit ($1/C_1=8.5$).

Fig. 21 Screw-type attractor of Fig. 12 together with the saddle-type periodic orbit ($1/C_1 = 8.8066$).

Fig. 22 Double-Scroll attractor of Fig. 13 together with the saddle-type periodic orbit ($1/C_1=9.0$).

Fig. 23 Attractor observed shortly before the boundary crisis ($1/C_1=10.5$). It is about to collide with the saddle-type periodic orbit.
periodic orbit.

Fig. 24 Cross section $v_{C_2}=0$ for the Poincare map of the saddle-type periodic orbit together with the stable and unstable eigen directions ($1/C_1=9.0$).

Fig. 25 Saddle-type periodic orbit survives even after the death of the attractor ($1/C_1=13.0$).

Fig. 26 Eventually passive resistor characteristic.

Fig. 27 One of two periodic orbits observed at G = 0.63.

Fig. 28 Period-2 orbit at G=0.64.

Fig. 29 Period-4 orbit at G=0.645.

Fig. 30 Spiral-type attractor at G=0.65.

Fig. 31 Double-scroll attractor at G=0.68.

Fig. 32 Asymmetric periodic window at G=0.7498. Another periodic attractor located symmetrically with respect to origin is also present.

Fig. 33 Period-2 version of Fig 32 at G=0.75.

Fig. 34 Ribbon-like attractor at G=0.751. Another attractor located symmetrically with respect to the origin is also present.

Fig. 35 Period-2 window at G=0.753.

Fig. 36 Periodic window at G=0.7535.

Fig. 37 Double-Scroll attractor at G=0.766.

Fig. 38 Ribbon-like attractor at G=0.7694. Another attractor located symmetrically with respect to origin is also present.

Fig. 39 Periodic window at G=0.77.

Fig. 40 Spiral attractor at G=0.773.

Fig. 41 Period-4 attractor at G=0.784.

Fig. 42 Period-2 attractor at G=0.791.

Fig. 43 Periodic attractor at G=0.795.

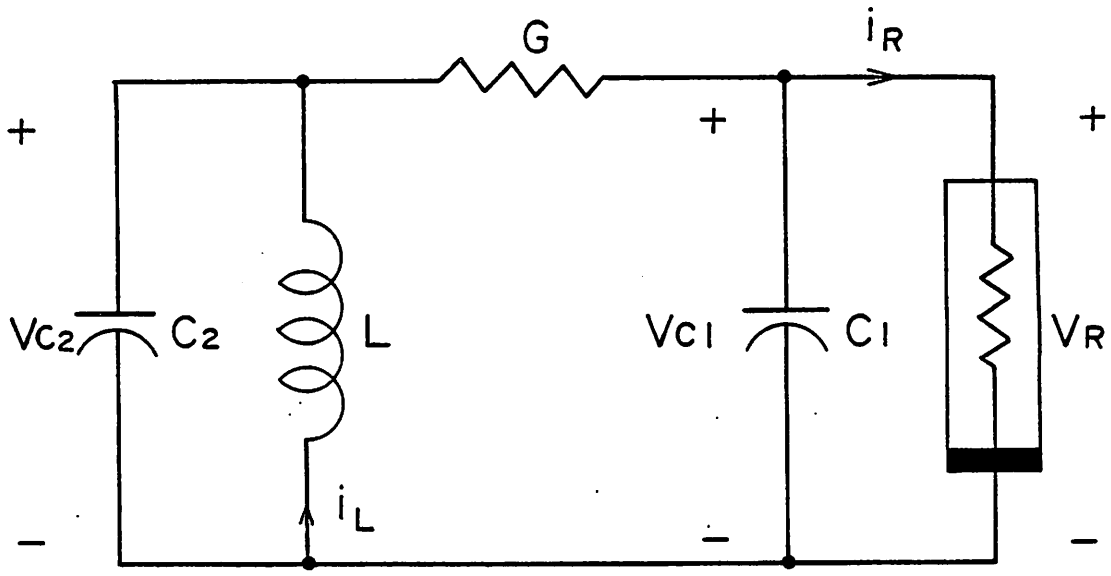

(a)

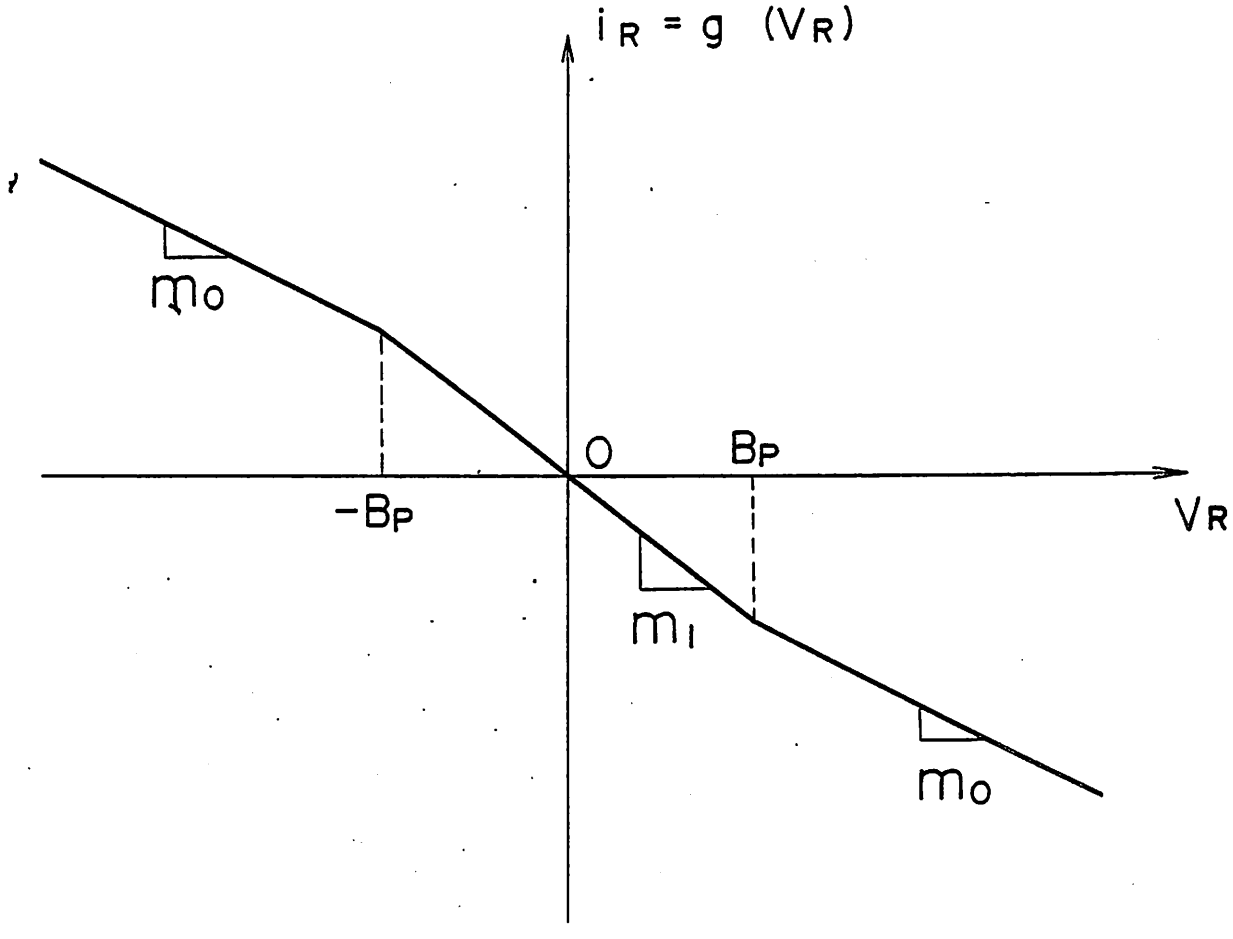

(b)

Fig. 1

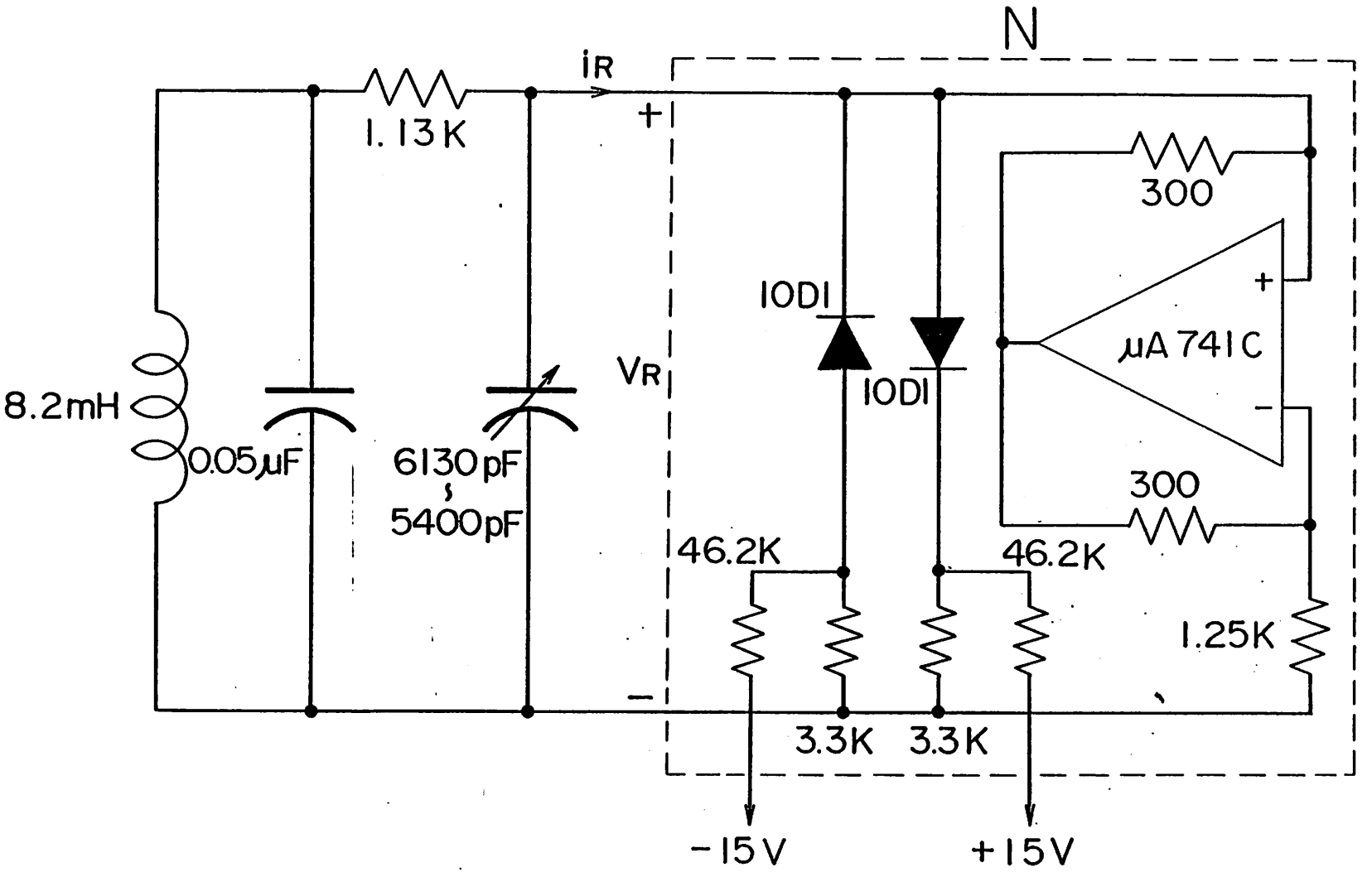
N
iR
1.13K
+
300
10D1
μA 741C
8.2mH
0.05μF
VR
6130pF
5400pF
10D1
300
46.2K
46.2K
1.25K
−
3.3K
3.3K
−15V
+15V

Fig. 2 (a)

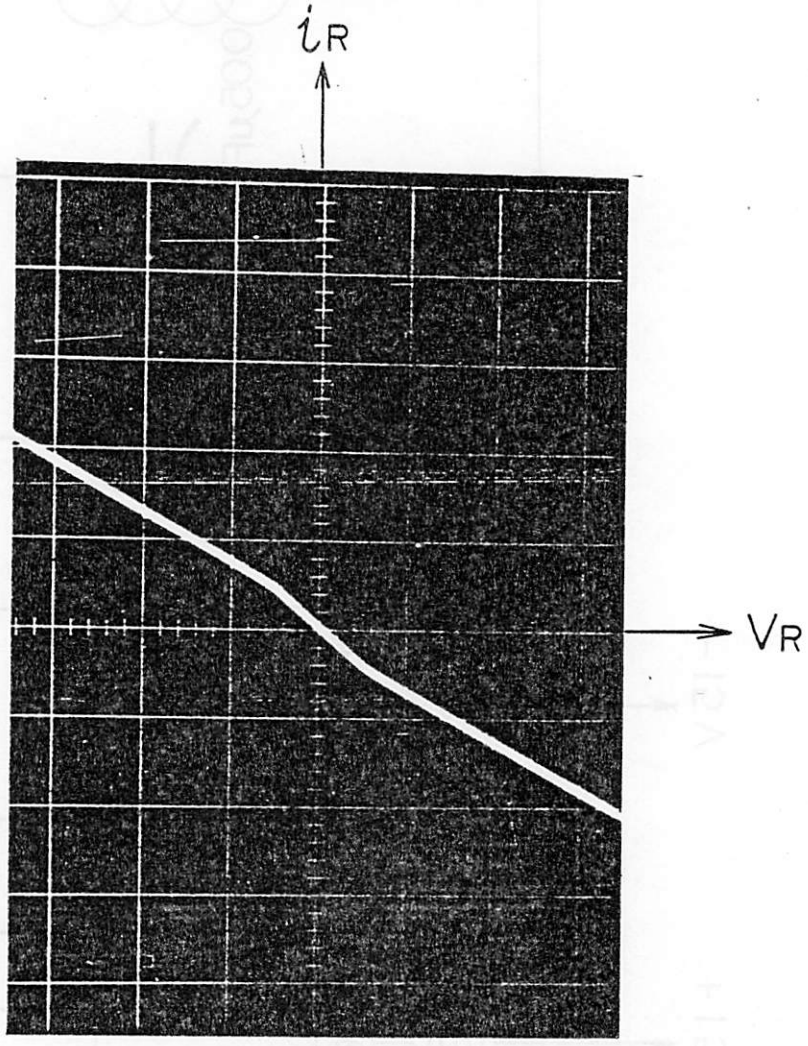

Fig. 2 (b)

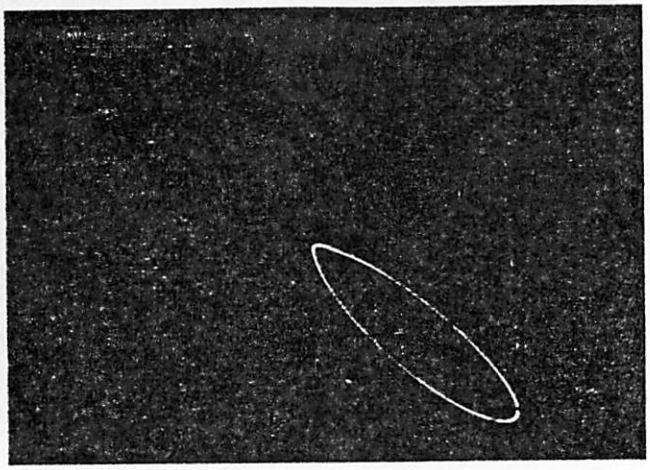

(a)

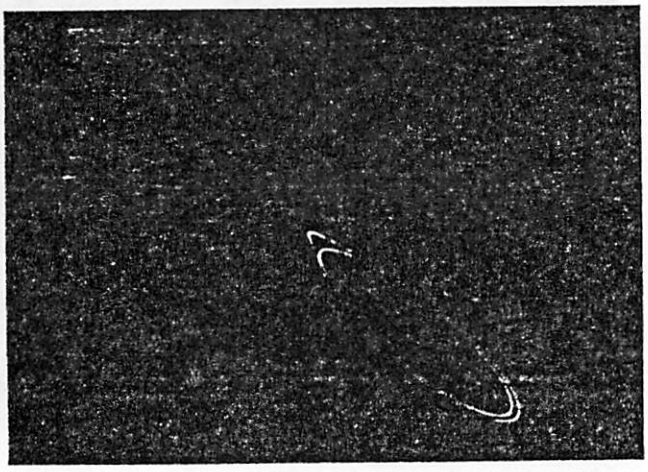

(b)

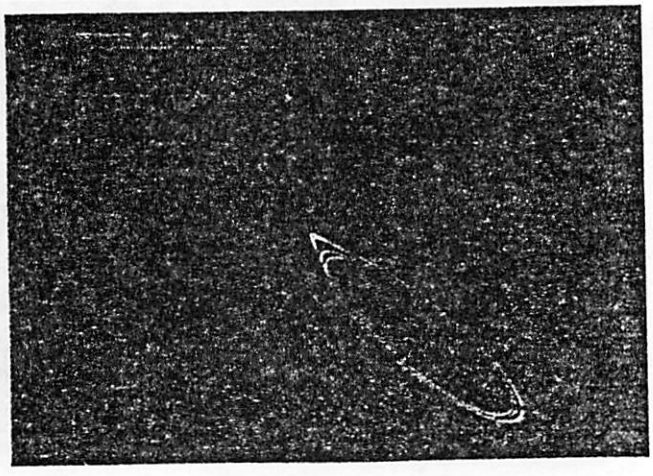

(c)

Fig. 3

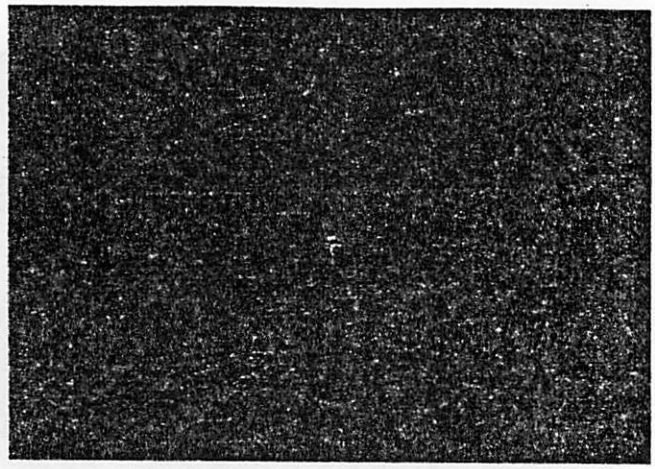

(d)

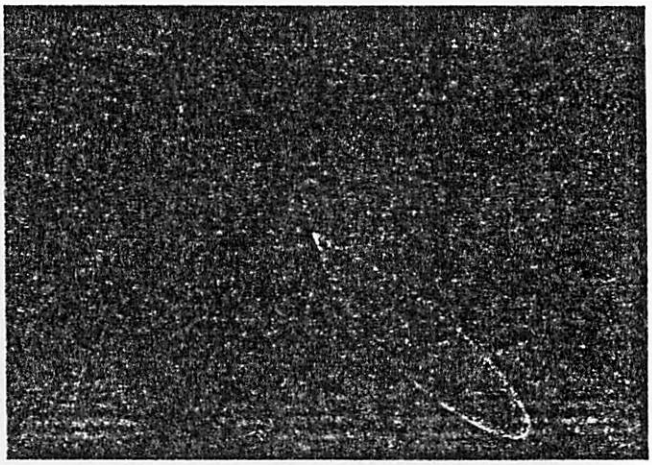

(e)

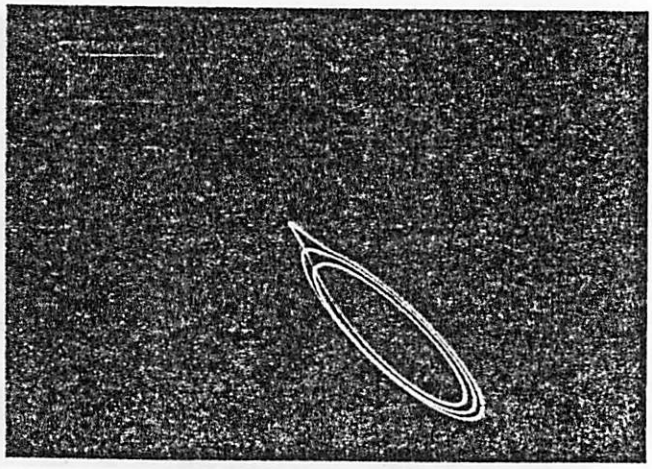

(f)

Fig. 3

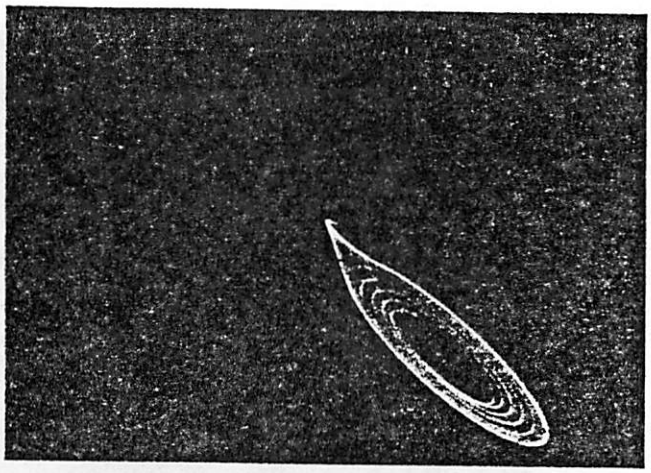

(g)

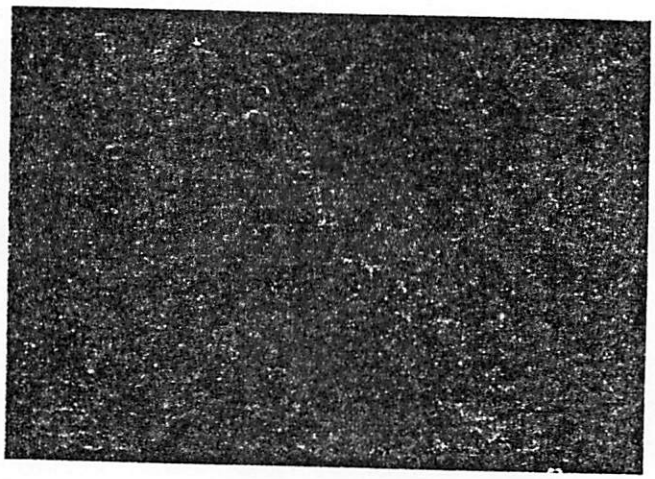

(h)

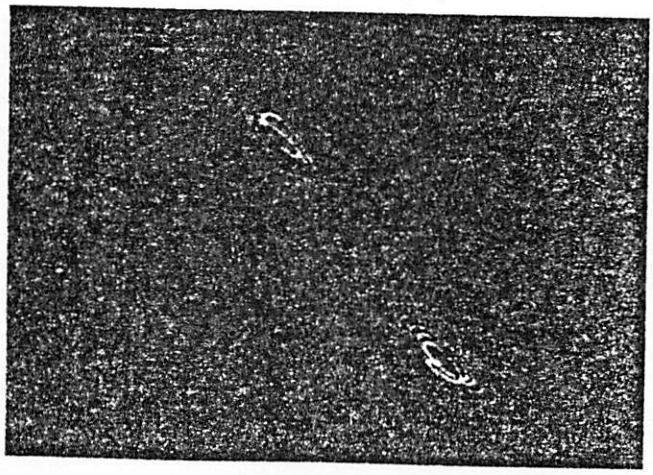

(i)

Fig. 3

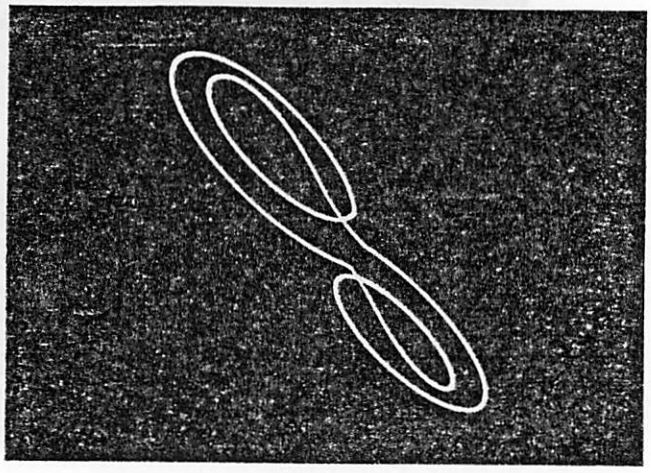

(j)

Fig. 3

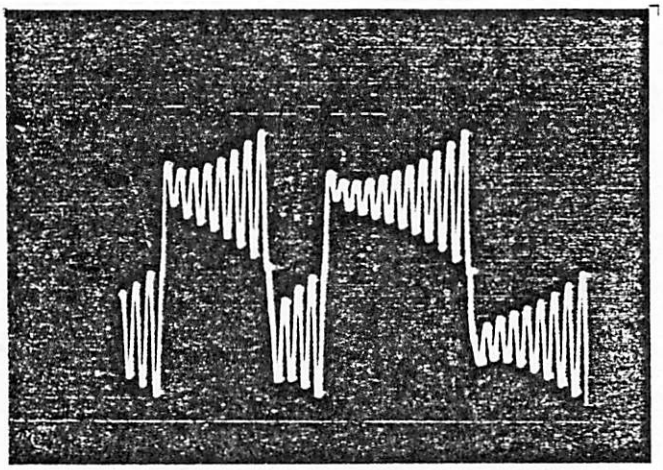

(a)

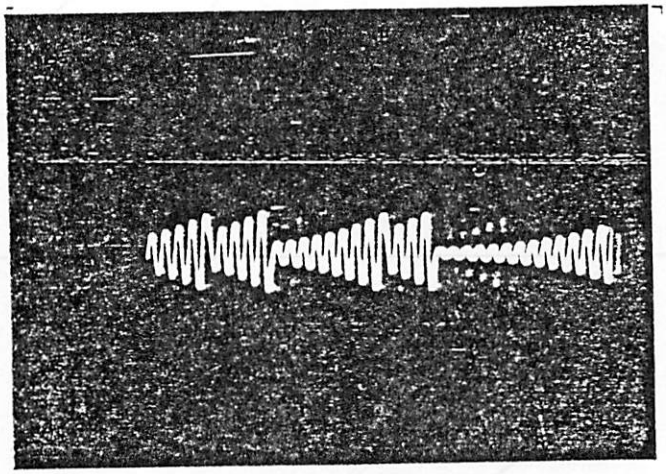

(b)

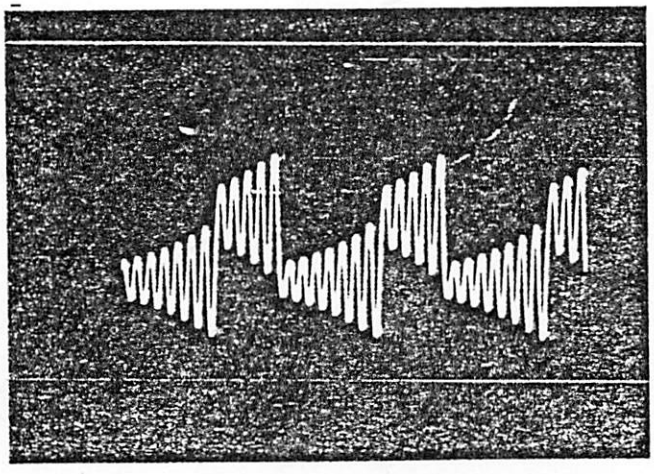

(c)

Fig. 1

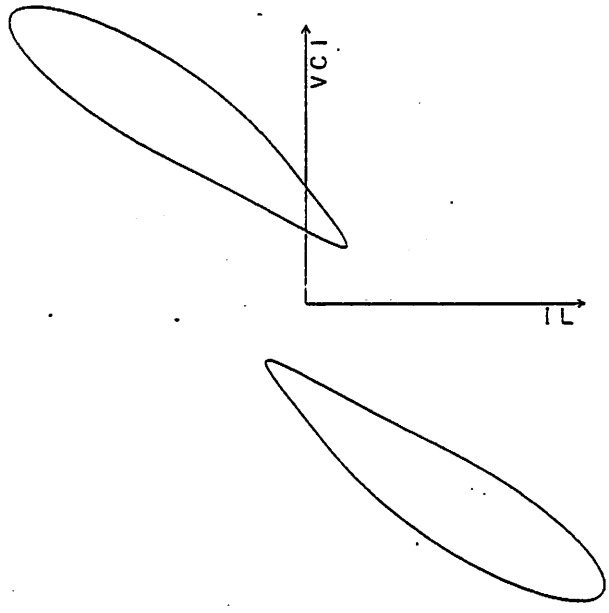

Fig. 5

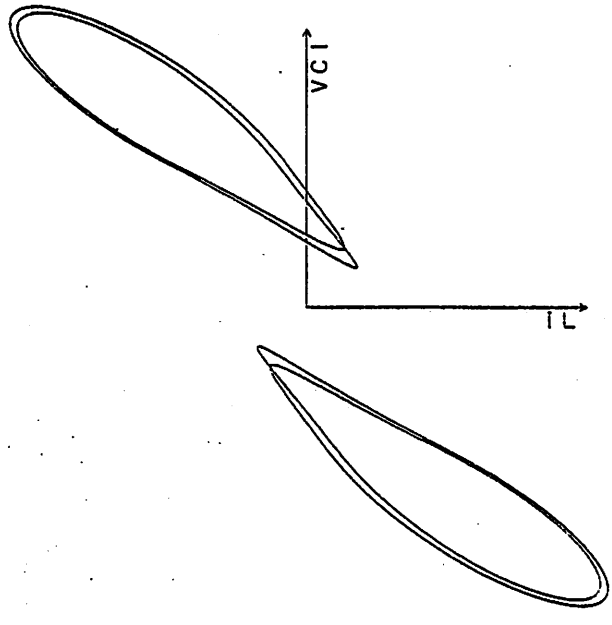

Fig. 6

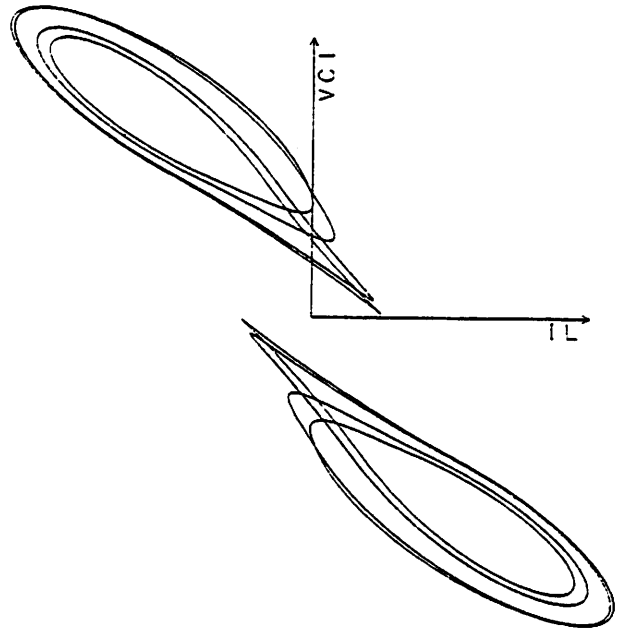

Fig. 7

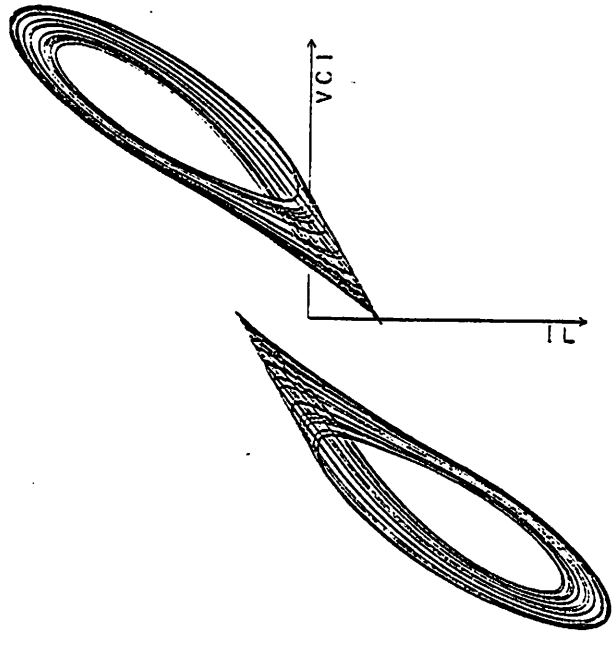

Fig. 8

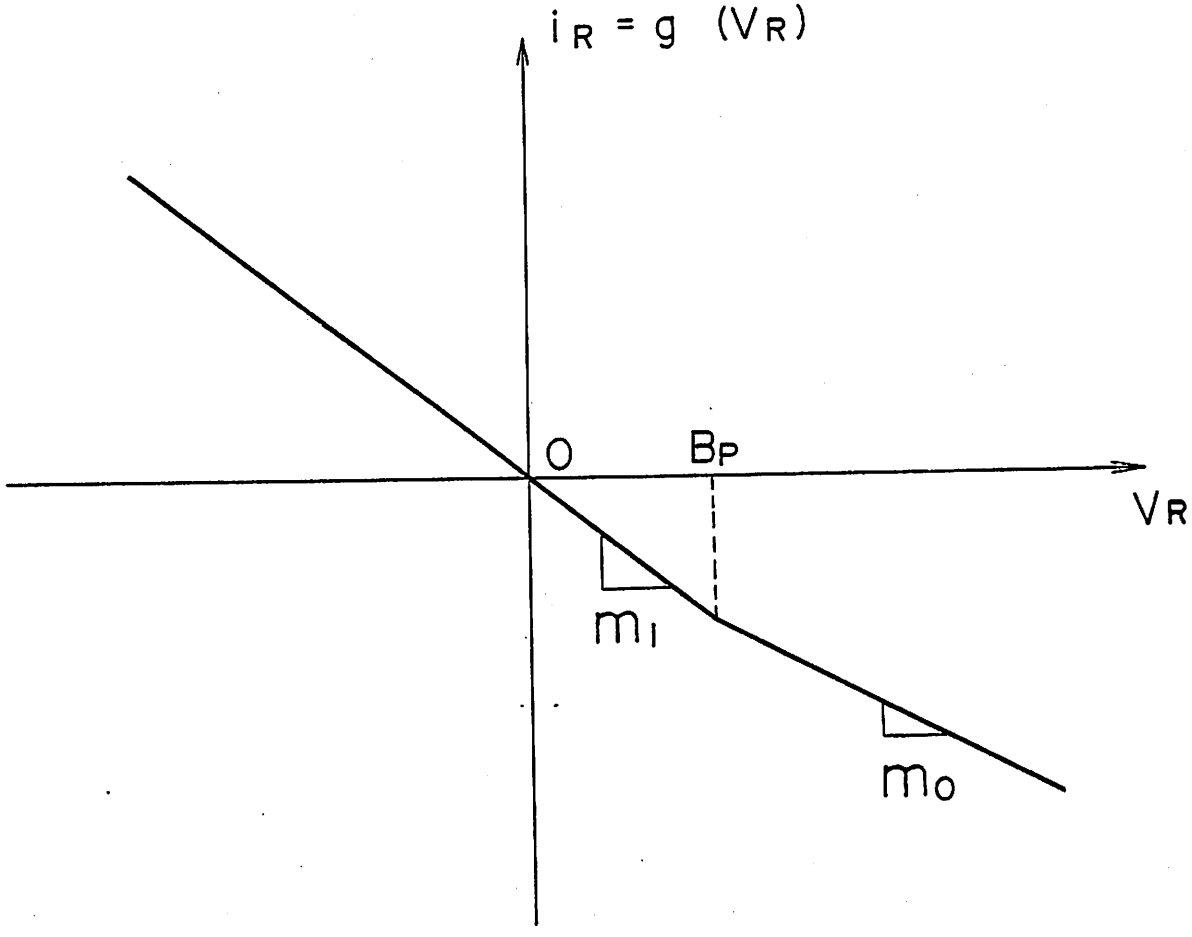

Fig. 9

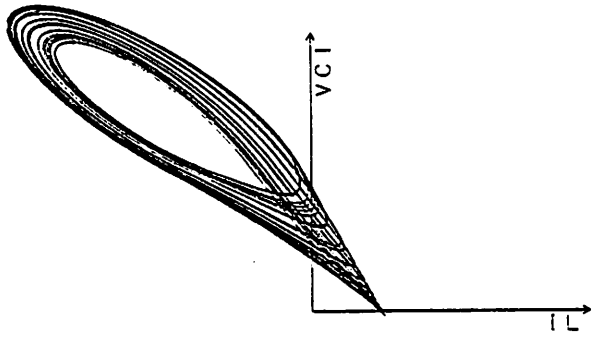

Fig. 10

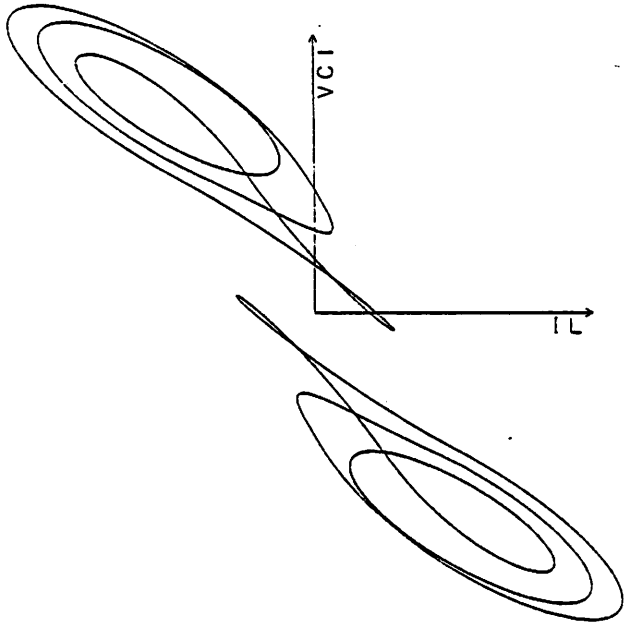

Fig. 11

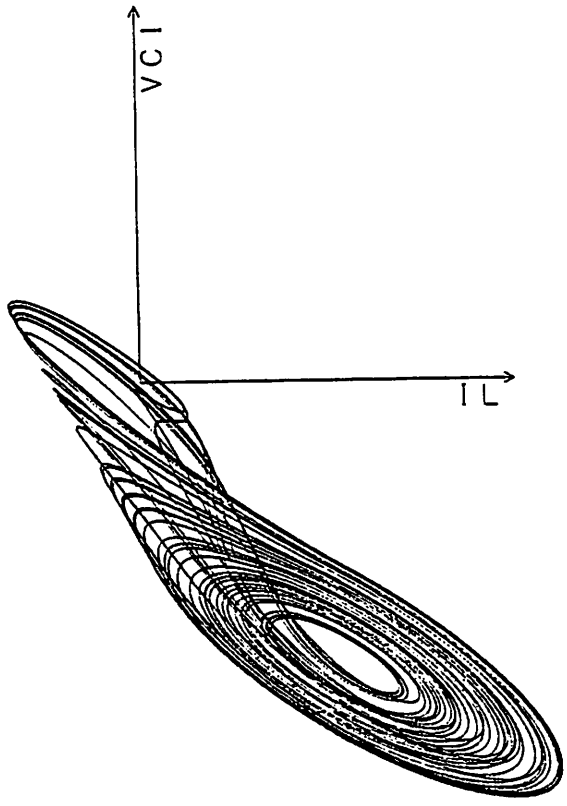

Fig. 12

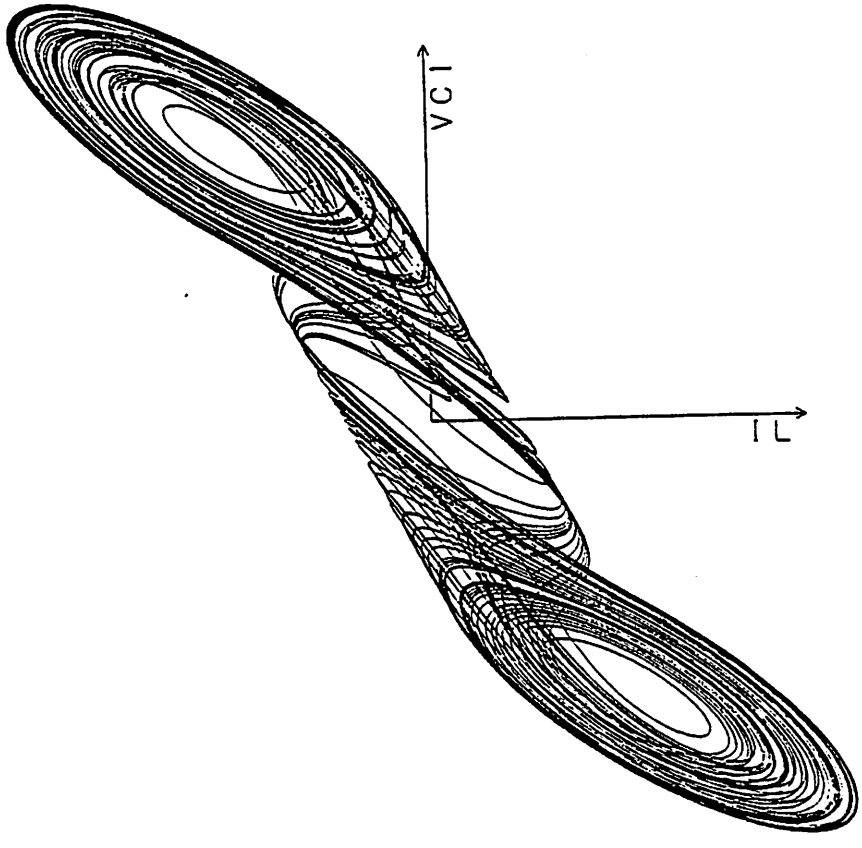

Fig. 13

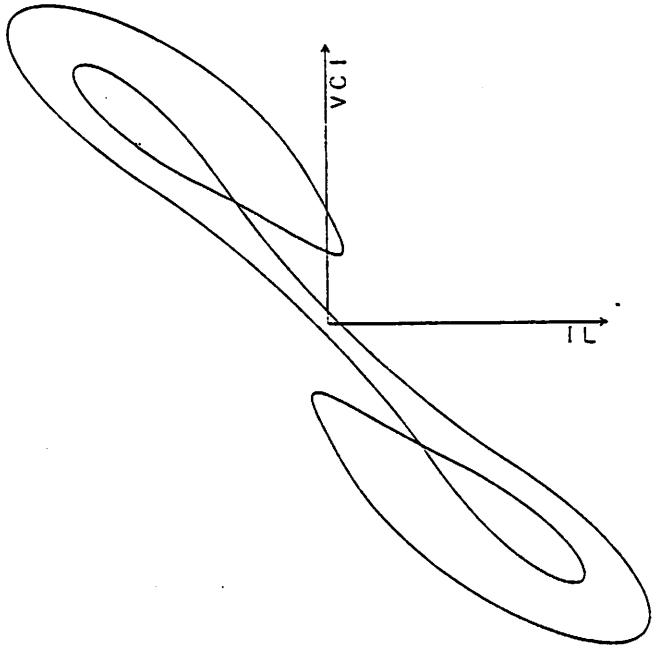

Fig. 14

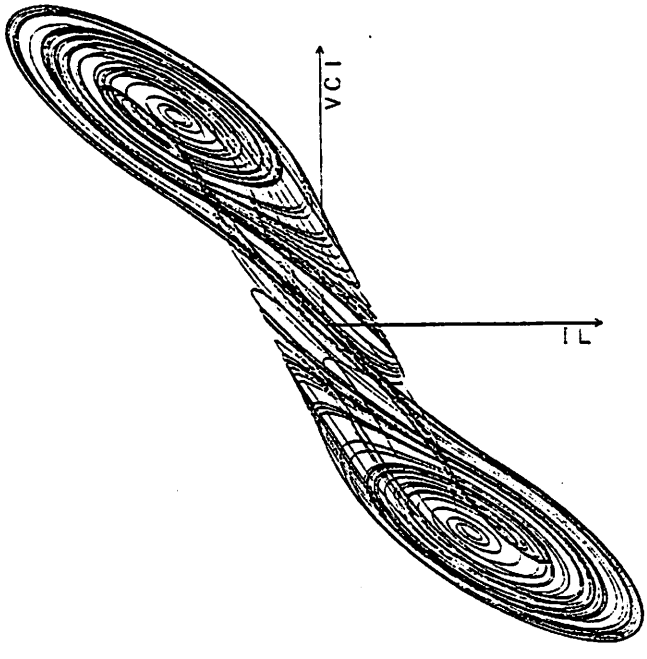

Fig. 15

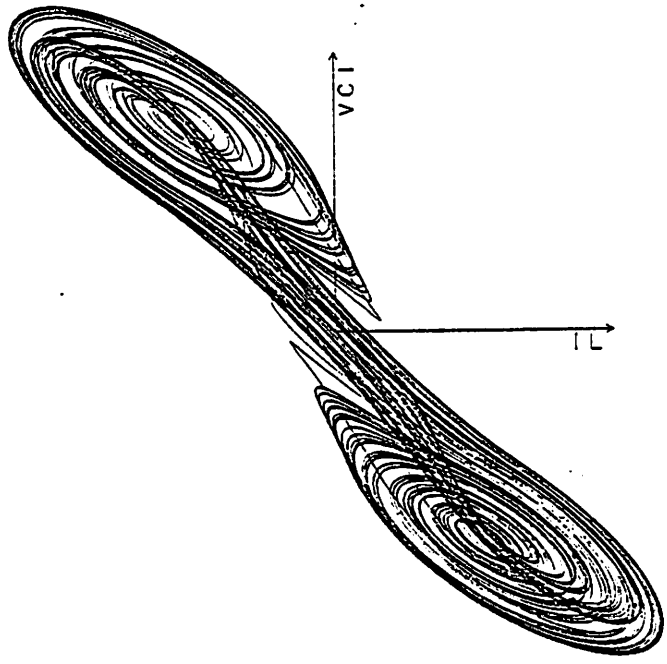

Fig. 16

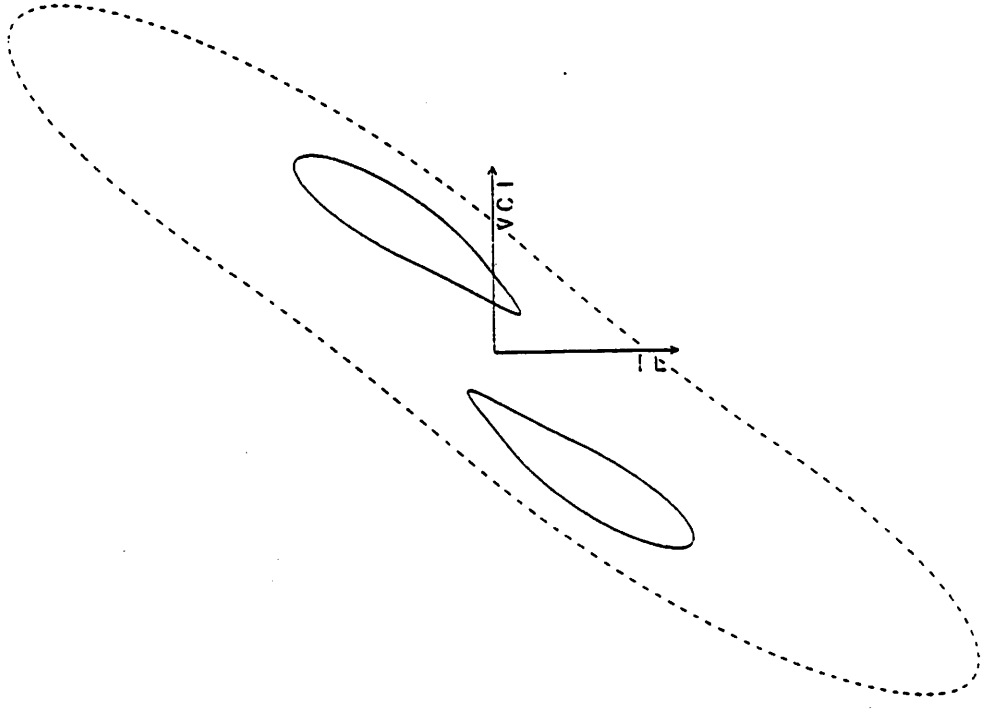

Fig. 17

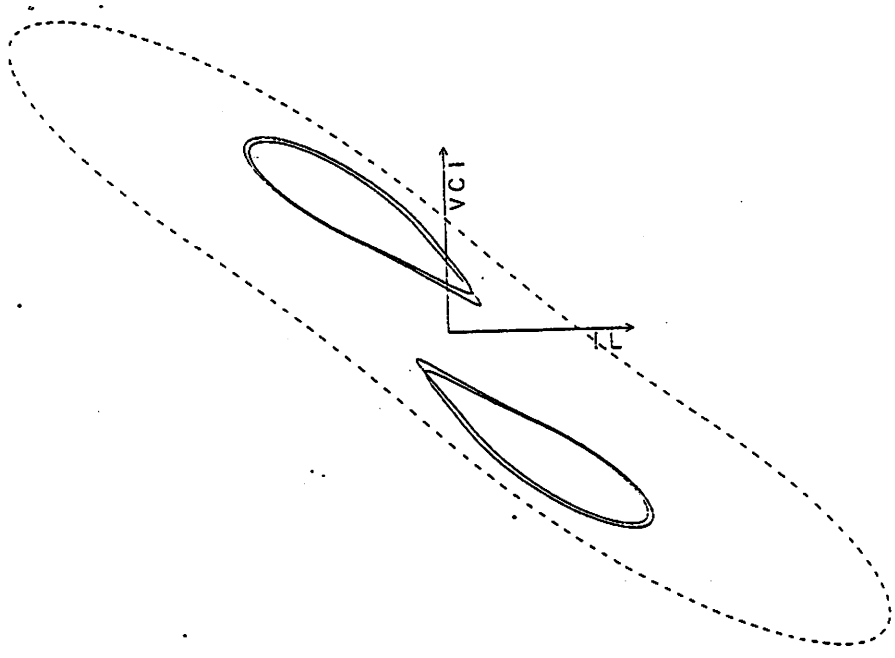

Fig. 18

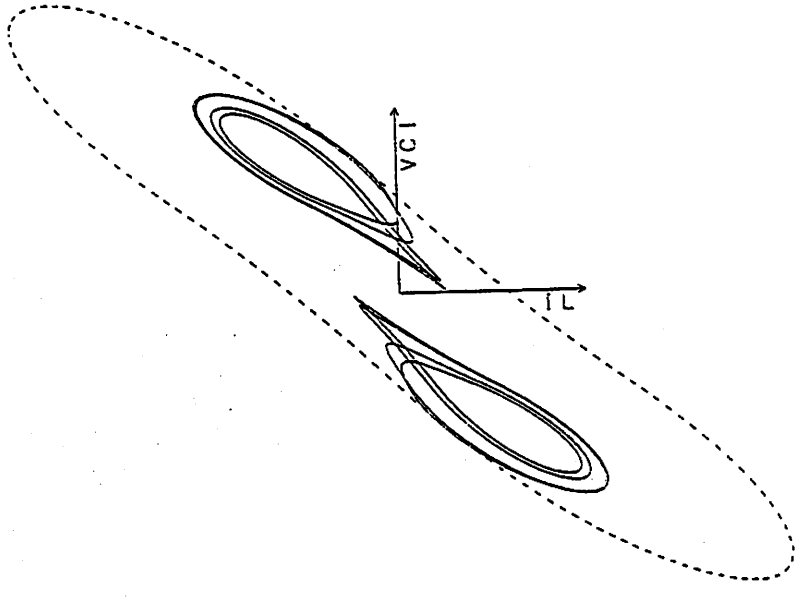

Fig. 19

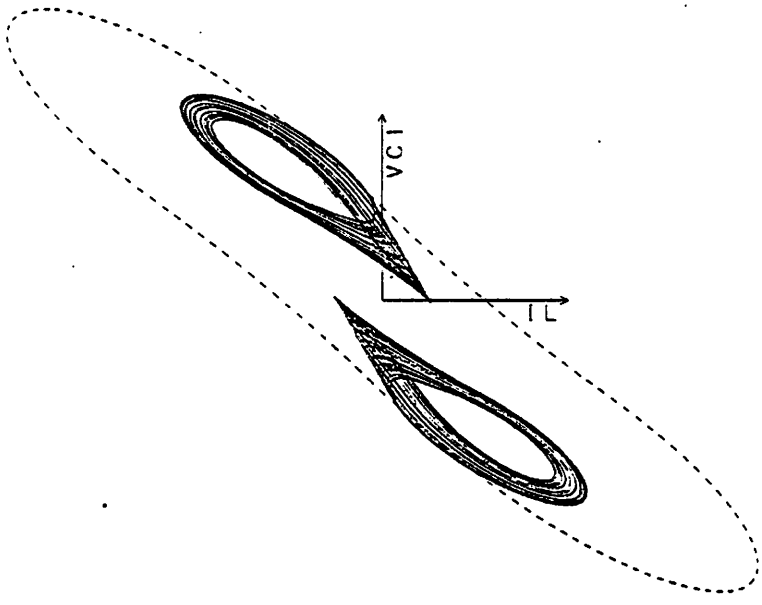

Fig. 20

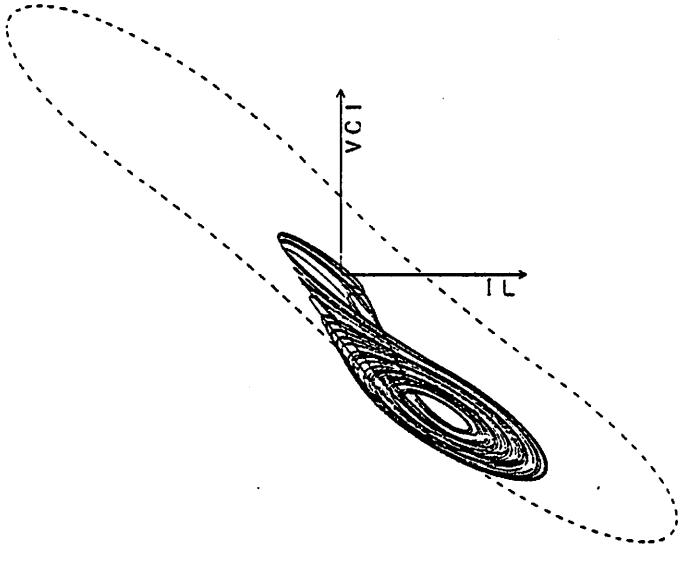

Fig. 21

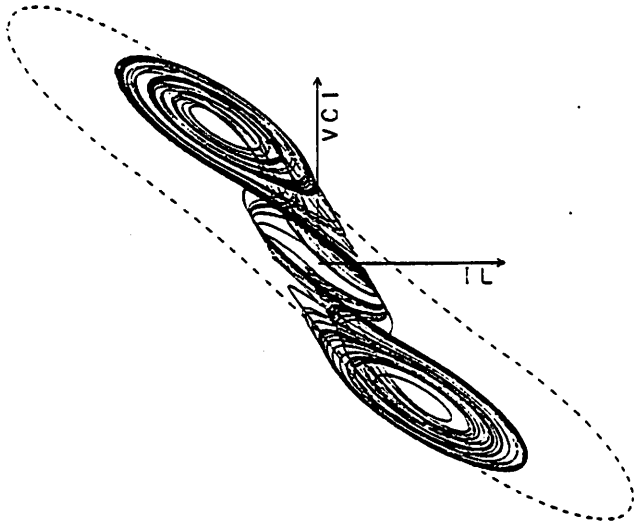

Fig. 22

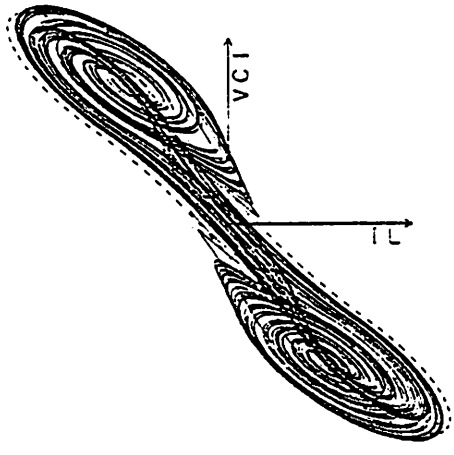

Fig. 23

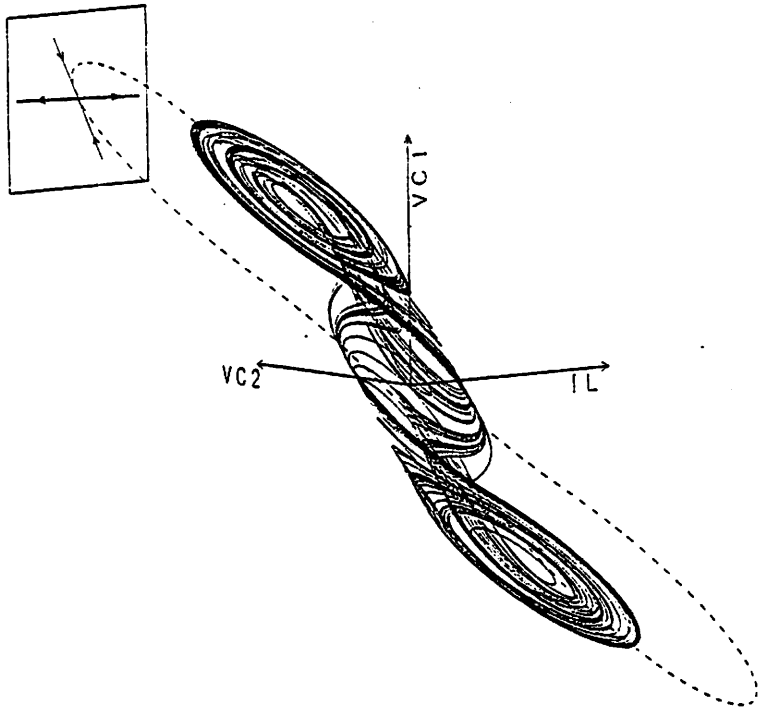

Fig. 24

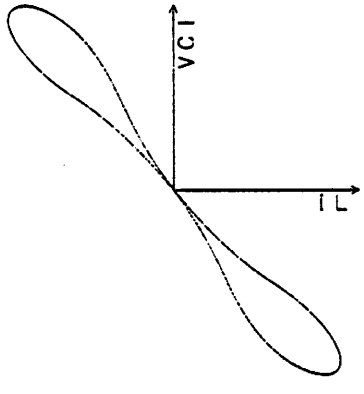

Fig. 25

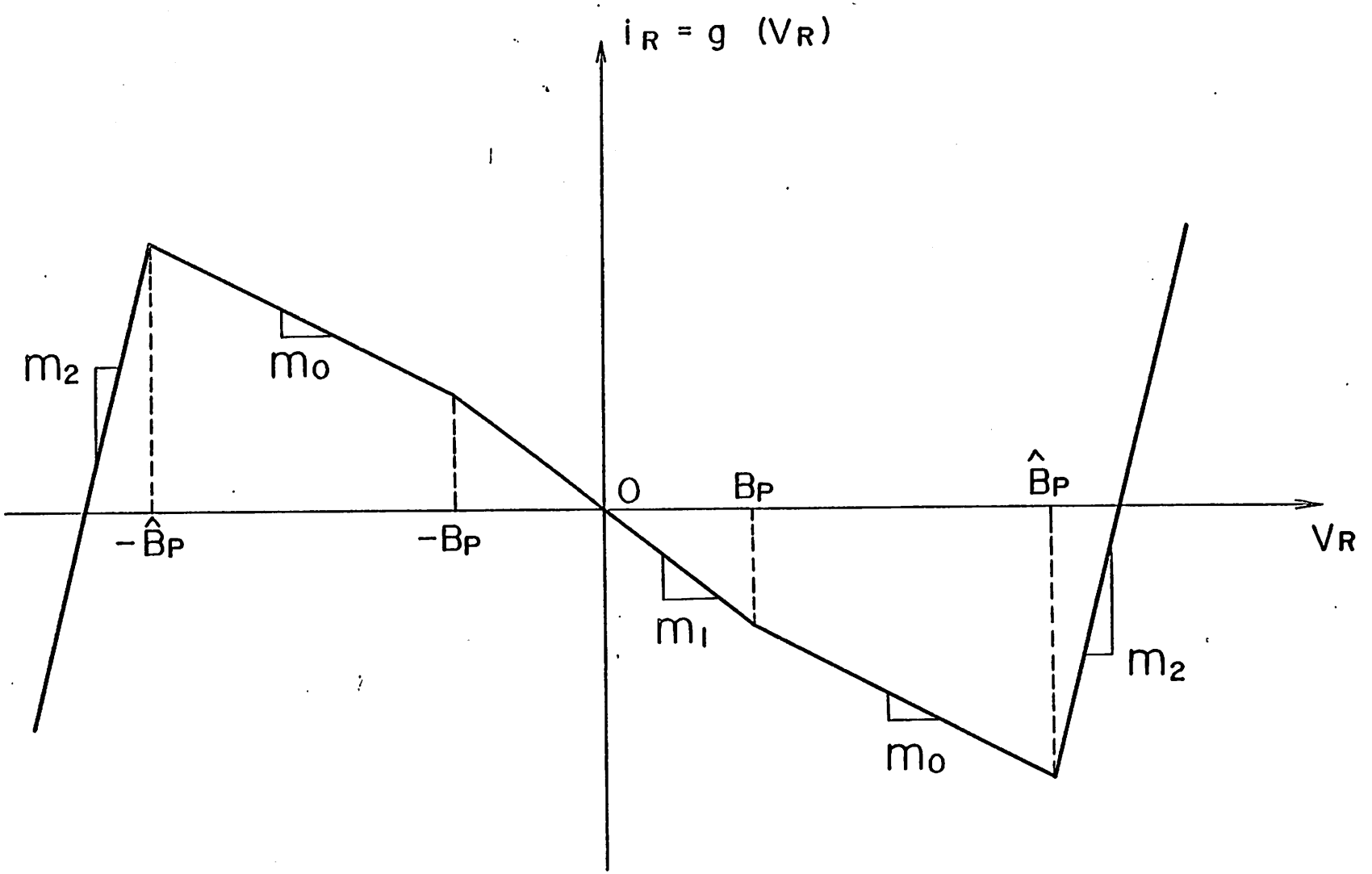

Fig. 26

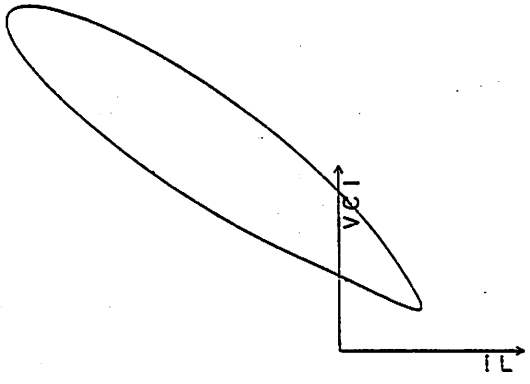

Fig. 27

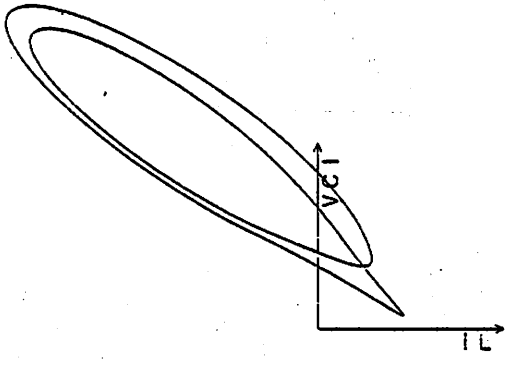

Fig. 28

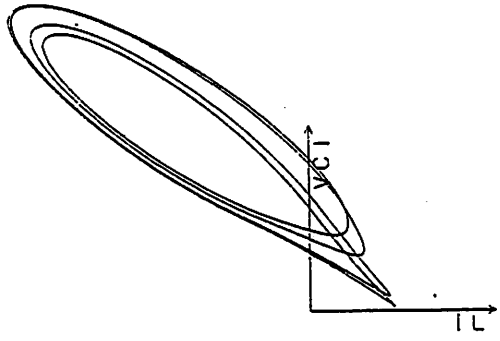

Fig. 29

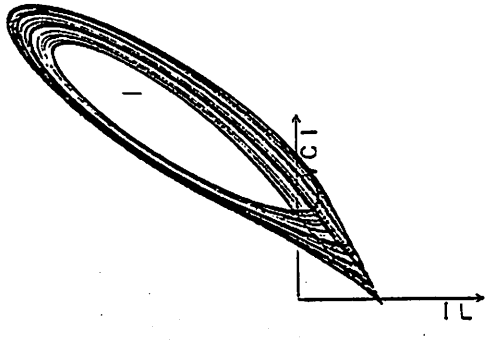

Fig. 30

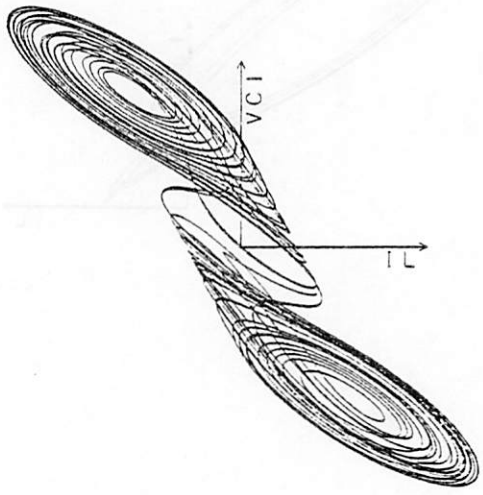

Fig. 31

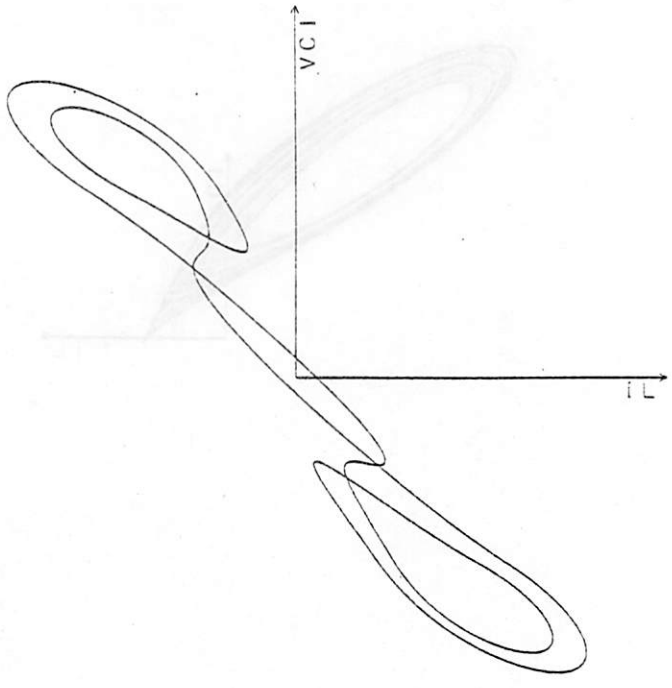

Fig. 32

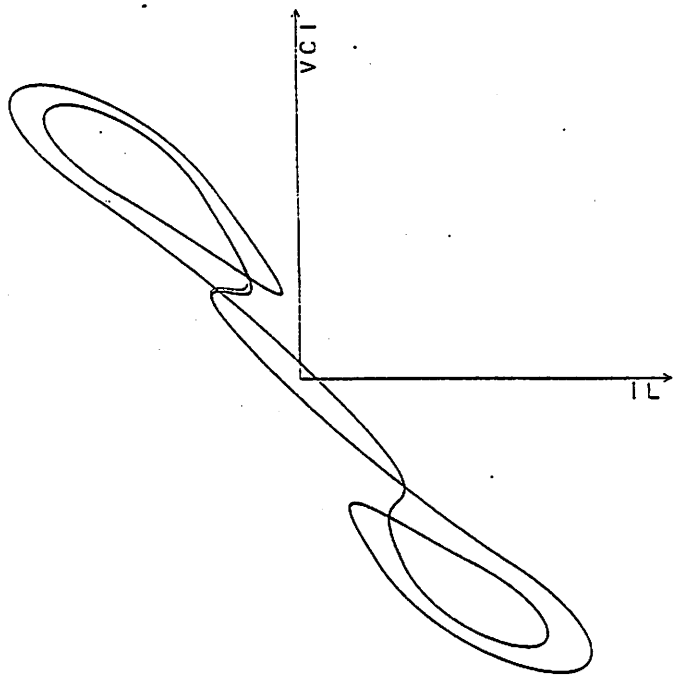

Fig. 33

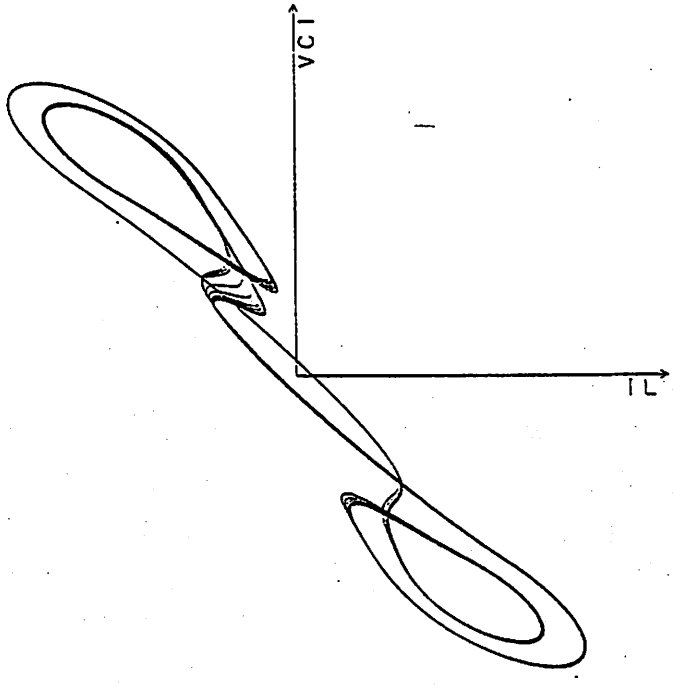

Fig. 34

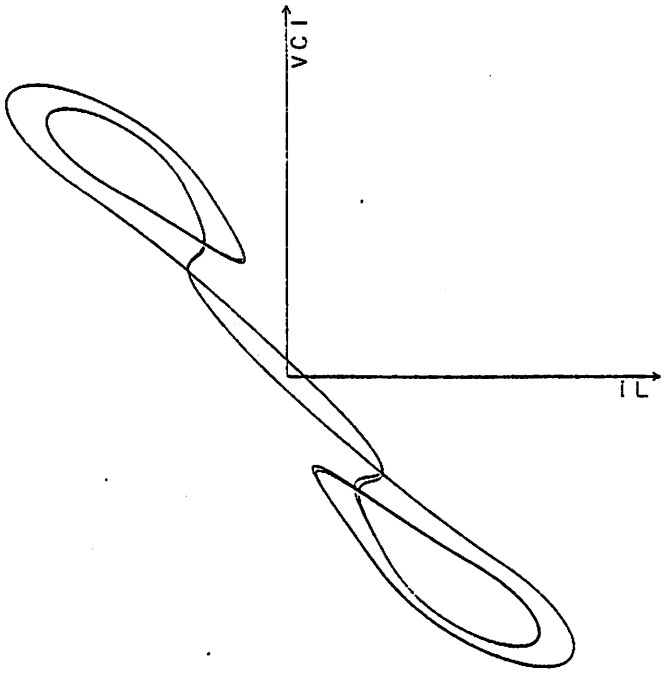

Fig. 35

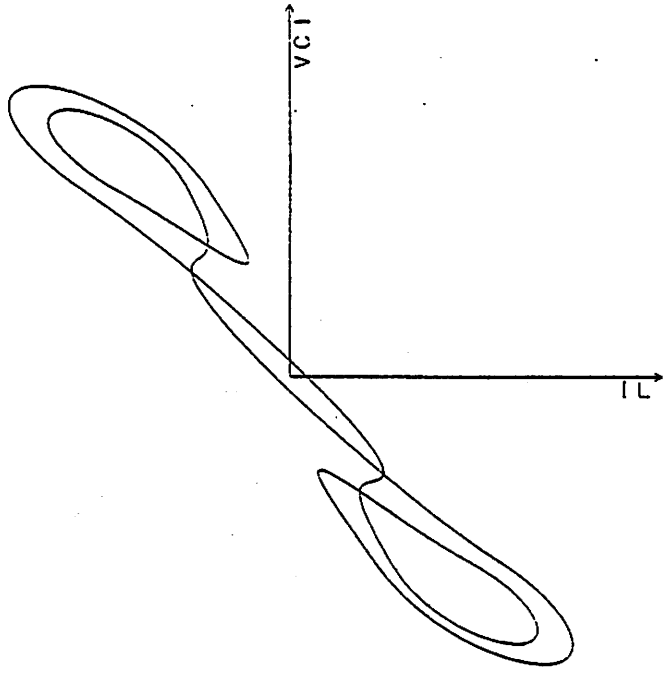

Fig. 36

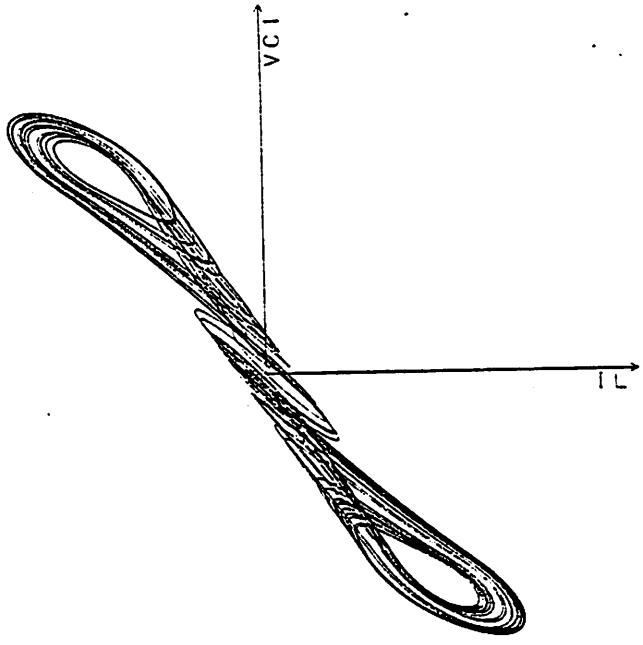

Fig. 37

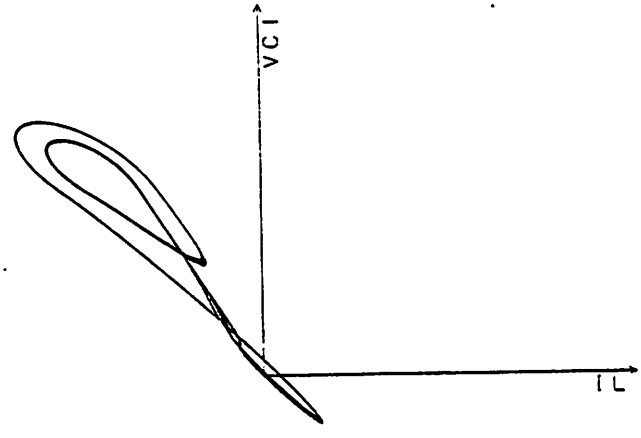

Fig. 38

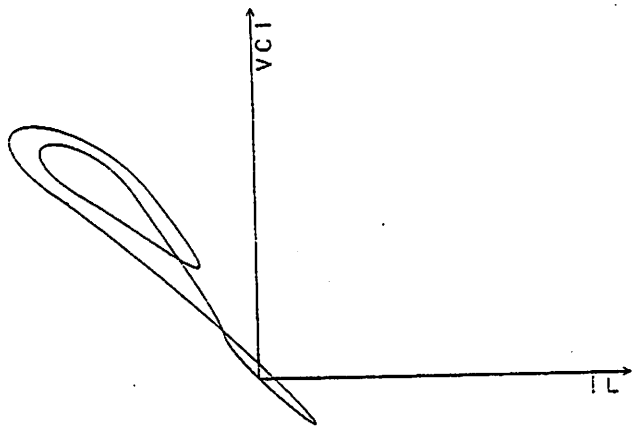

Fig. 39

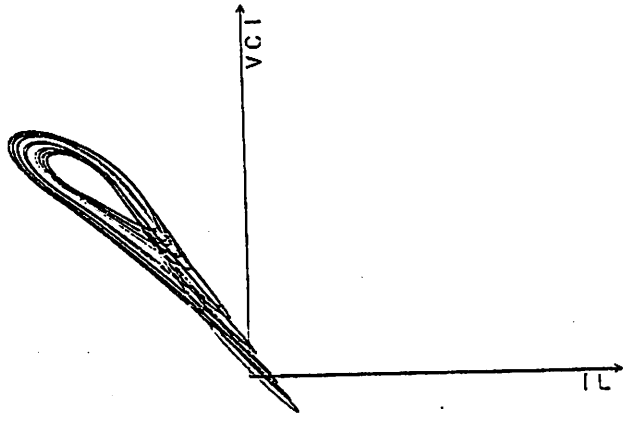

Fig. 40

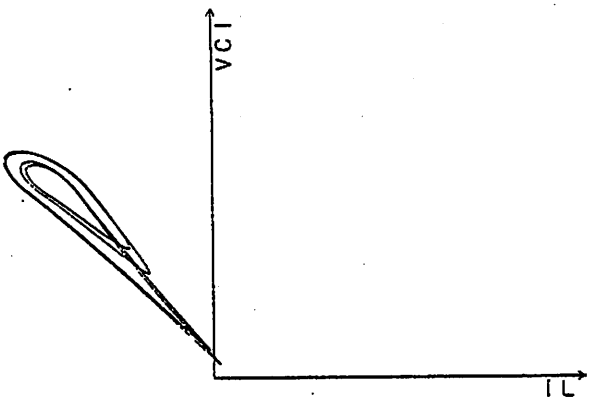

Fig. 41

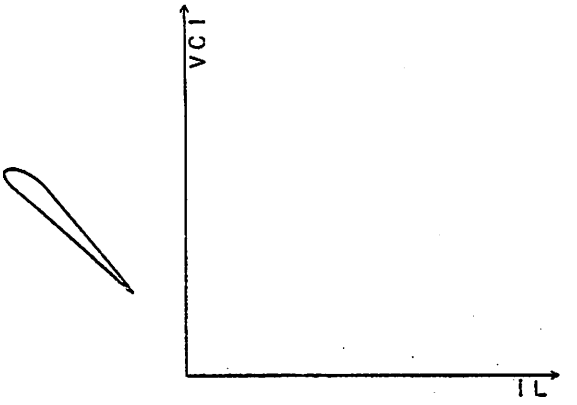

Fig. 42

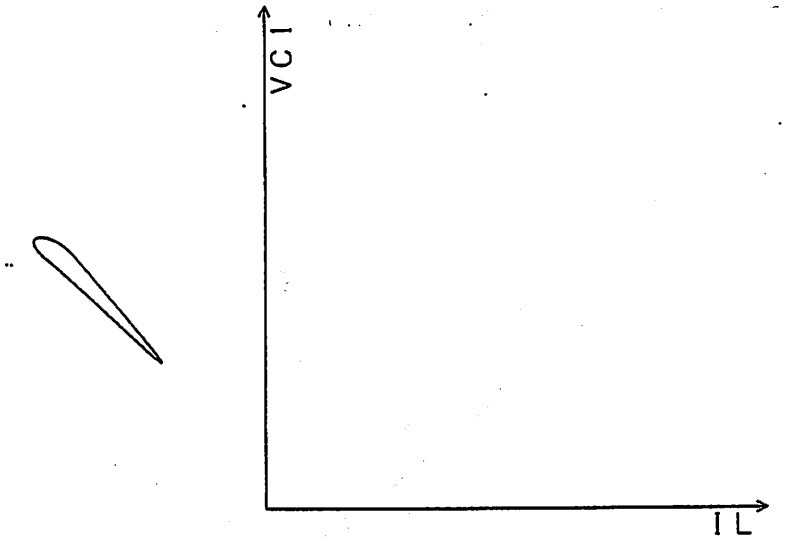

Fig. 43